EPJ A
Hadrons and Nuclei

EPJ.org
your physics journal

Eur. Phys. J. A (2017) **53**: 159 DOI 10.1140/epja/i2017-12347-9

Comprehensive overview of the Point-by-Point model of prompt emission in fission

A. Tudora and F.-J. Hambsch

Società Italiana di Fisica

Springer

Eur. Phys. J. A (2017) **53**: 159
DOI 10.1140/epja/i2017-12347-9

THE EUROPEAN PHYSICAL JOURNAL A

Regular Article – Theoretical Physics

Comprehensive overview of the Point-by-Point model of prompt emission in fission

A. Tudora[1,a] and F.-J. Hambsch[2]

[1] University of Bucharest, Faculty of Physics, 405 Atomistilor Str., POB MG-11, R0-77125, Bucharest Magurele, Romania
[2] European Commission, Joint Research Centre, Directorate G – Nuclear Safety and Security, Unit G2, Retieseweg 111, B-2440, Geel, Belgium

Received: 15 February 2017 / Revised: 10 July 2017
Published online: 3 August 2017 – © Società Italiana di Fisica / Springer-Verlag 2017
Communicated by F. Gulminelli

Abstract. The investigation of prompt emission in fission is very important in understanding the fission process and to improve the quality of evaluated nuclear data required for new applications. In the last decade remarkable efforts were done for both the development of prompt emission models and the experimental investigation of the properties of fission fragments and the prompt neutrons and γ-ray emission. The accurate experimental data concerning the prompt neutron multiplicity as a function of fragment mass and total kinetic energy for ^{252}Cf(SF) and ^{235}U(n,f) recently measured at JRC-Geel (as well as other various prompt emission data) allow a consistent and very detailed validation of the Point-by-Point (PbP) deterministic model of prompt emission. The PbP model results describe very well a large variety of experimental data starting from the multi-parametric matrices of prompt neutron multiplicity $\nu(A,TKE)$ and γ-ray energy $E_\gamma(A,TKE)$ which validate the model itself, passing through different average prompt emission quantities as a function of A (*e.g.*, $\nu(A)$, $E_\gamma(A)$, $\langle\varepsilon\rangle(A)$ etc.), as a function of TKE (*e.g.*, $\nu(TKE)$, $E_\gamma(TKE)$) up to the prompt neutron distribution $P(\nu)$ and the total average prompt neutron spectrum. The PbP model does not use free or adjustable parameters. To calculate the multi-parametric matrices it needs only data included in the reference input parameter library RIPL of IAEA. To provide average prompt emission quantities as a function of A, of TKE and total average quantities the multi-parametric matrices are averaged over reliable experimental fragment distributions. The PbP results are also in agreement with the results of the Monte Carlo prompt emission codes FIFRELIN, CGMF and FREYA. The good description of a large variety of experimental data proves the capability of the PbP model to be used in nuclear data evaluations and its reliability to predict prompt emission data for fissioning nuclei and incident energies for which the experimental information is completely missing. The PbP treatment can also provide input parameters of the improved Los Alamos model with non-equal residual temperature distributions recently reported by Madland and Kahler, especially for fissioning nuclei without any experimental information concerning the prompt emission.

1 Introduction

The investigation of prompt emission in fission is very important in understanding the fission process. For nuclear modeling and improved evaluations of nuclear fission data, the experimental investigation of the properties of fission fragments and prompt fission neutrons (*e.g.*, their multiplicities and energy distribution) can give answers to questions related to important aspects of the modeling of prompt emission (*e.g.*, formation of the fission fragments, sharing of the excitation energy among them).

In the last decade remarkable efforts were done in the development of prompt emission models. The actual probabilistic and deterministic models (see, *e.g.*, the comprehensive paper [1]) are able to provide various prompt emission quantities as a function of mass, charge and kinetic energy of the fragments. The reliability and the predictive power of these models can be supported only by a detailed and rigorous validation. The first and most important validation consists in the comparison of the model results with many and various prompt emission data correlated with the fragment properties.

In this sense the spontaneous fission of ^{252}Cf(SF) serves as an excellent benchmark of prompt emission in fission since experimental data can be obtained without the need of an incident neutron beam. Recently an experiment on ^{252}Cf(SF) has been performed at JRC-Geel [2] with the purpose of providing high-quality experimental

[a] e-mail: anabellatudora@hotmail.com

data of the prompt neutron multiplicity in correlation with fission fragment mass (A) and total kinetic energy (TKE).

These data offer the possibility of a more detailed validation of prompt emission models, in this case, of the deterministic model Point-by-Point (PbP). The comparison of the prompt neutron multiplicity matrix $\nu(A, TKE)$ of the PbP model with the experimental data of Göök *et al.* [2] is particularly relevant because the multi-parametric matrices of different prompt emission quantities, as primary results of the PbP model, do not depend on the fragment distribution. In other words the good agreement of the multi-parametric matrices of prompt emission quantities with available experimental data constitutes a validation of the model itself.

The comparison with experimental data of different average prompt emission quantities, *i.e.* as a function of fragment mass, as a function of TKE and total average quantities, implies the use of fragment distributions over which the multi-parametric matrices are averaged. Consequently, the good description of these data depends, not only on the modeling itself, but also on the reliability of the fragment distributions.

In recent years comparisons of a part of the PbP model results with the experimental data available at that time for different fissioning nuclei were reported. In the mean time, new experimental data have become available. They refer on one side to the prompt emission (*e.g.*, the data reported by Göök *et al.* [2,3]) and, on the other hand, to fission fragment distributions recently measured (*e.g.*, the data of ref. [4] for ^{235}U(n_{th}, f) and the $Y(A, TKE)$ data of Göök for ^{252}Cf(SF)). These new data allow a more detailed validation of the PbP model (which also was improved in the mean time, *e.g.* concerning the deterministic construction of the fragmentation range).

Moreover, in the case of ^{252}Cf(SF) the validation based on different average data reported in ref. [2] is entirely consistent. Because the average prompt emission quantities (*e.g.*, as a function of A or as a function of TKE) were obtained by averaging the corresponding multi-parametric matrices provided by the PbP model over the fragment distribution $Y(A, TKE)$ of the same experiment of Göök *et al.*

Starting from the aspects mentioned above, the present paper includes a comprehensive comparison of the PbP model results as multi-parametric matrices and as different average quantities (based on new experimental fragment distributions) especially with the recent experimental data, *e.g.*, refs. [2,3], and in some cases with the results of other models, too. As standard fissioning systems ^{252}Cf(SF) and ^{235}U(n_{th}, f), benefiting of the most accurate and numerous experimental data, were chosen for this study. The comparison is organized in subsections for each type of quantities, *e.g.* multi-parametric matrices, average quantities as a function of A, average quantities as a function of TKE, the prompt neutron distribution $P(\nu)$ etc.

Even if the main features of the PbP model were presented separately in previous papers and were concisely mentioned in ref. [1], in order to make the present paper more easily readable, a short description of the entire PbP model is given in a separate section.

As it was mentioned in ref. [1], a milestone in the theoretical investigation of the shape of the total average prompt neutron spectra in the laboratory frame was the Los Alamos (LA) model published in 1982 by Madland and Nix [5]. This model with subsequent improvements has become the workhorse underlying modern prompt neutron spectrum evaluations.

Very recently Madland and Kahler [6] proposed a refined LA model. The improvement consists in the consideration of non-equal maximum temperatures T_m (of the residual temperature distribution $P(T)$ with a triangular form) for the light and heavy fragments of the most probable fragmentation. The capability of this improved LA model in the description of experimental prompt neutron spectra of ^{252}Cf(SF) and ^{235}U(n_{th}, f) is demonstrated in ref. [6] by the use of input model parameters that are based on the experimental data of prompt neutron multiplicity and prompt γ-ray energy as a function of fragment mass, $\nu(A)$ and $E_\gamma(A)$.

As in the case of the classical LA model of Madland and Nix [5] (considering equal T_m of both fragments) for which the PbP treatment was the basis of the developed systematic of its input parameters [7] again the PbP treatment can assure reliable input parameters for the new LA model with non-equal T_m without the need of experimental $\nu(A)$ and $E_\gamma(A)$ data. Results of the new LA model with non-equal T_m using input parameters provided by the PbP treatment are given in the last subsection.

2 Description of the PbP model

2.1 The fragmentation range

The fragmentations (*i.e.*, pairs of fragments) that are taken into account, forming the so-called fragmentation range, play a crucial role in the PbP treatment.

The fragmentation range is constructed in a deterministic way as follows. The range of fragment mass numbers A is taken from the symmetric fission up to a very asymmetric split (with a step of 1 mass unit). Three or five charge numbers Z are considered at each A, as the nearest integers above and below the most probable charge Z_p. This is taken as the unchanged charge distribution (UCD) corrected with the charge polarization $Z_p(A) = Z_{UCD}(A) + \Delta Z(A)$. Charge deviations either as a function of A (oscillating with a periodicity of about 5 mass units in the asymmetric fission region, as experimental data or provided by the Z_p model [8]), or the same value $\Delta Z = |0.5|$ (with the + sign for light fragments and the minus sign for the heavy fragments) can be considered. The charge distributions at each A, $p(Z, A)$, are taken as Gaussian functions centered on Z_p either with root-mean-squares as a function of A, $rms(A)$, also oscillating with a periodicity of about 5 mass units or with the same $rms = 0.6$ (when ΔZ is taken $|0.5|$).

As it was mentioned in ref. [9] the mean values of ΔZ and rms, obtained by averaging $\Delta Z(A)$ and $rms(A)$ over the fragment mass distributions $Y(A)$, are of about

0.5 and 0.6 respectively, for all fissioning systems studied (^{233,235}U(n_{th},f), ^{234}U(n,f), ^{239}Pu(n_{th},f), ^{252}Cf(SF), $^{236-244}$Pu(SF)). Details about the charge polarization and the isobaric charge distribution, in connection with the even-odd effects in fragment distributions and prompt emission, can be found, *e.g.*, in refs. [10–12] and references therein. In the absence of $\Delta Z(A)$ information, the use of the average values $\Delta Z = |0.5|$ and $rms = 0.6$ for all A is a satisfactory approximation [9].

For each fragmentation determined as mentioned above, prompt emission calculations are done at TKE values covering a large range (*e.g.*, from 100 MeV to 200 MeV) usually with a step of 5 MeV.

2.2 Fragment excitation energies and level density parameters at scission and at full acceleration

Once the fragmentation range is constructed, the energy release (Q-value) of each pair of fragments is easily calculated using the mass excesses from nuclear data libraries (*e.g.*, of Audi and Wapstra taken from RIPL3 [13]). The total excitation energy (TXE) of each fragmentation at each TKE value (covering the fragmentation range described in sect. 2.1) is also calculated as $TXE(A,Z,TKE) = Q(A,Z) + E_n + B_n - TKE$, in which B_n and E_n are the neutron binding energy and the incident neutron energy in the case of neutron-induced fission (n,f). In the case of spontaneous fission (SF) both B_n and E_n are zero.

The excitation energy at full acceleration of the complementary fragments of each fragmentation is obtained from a TXE partition method based on modeling at scission. This method was described in detail in refs. [14,15]. Briefly this modeling at scission consists in the calculation of the extra-deformation energy ΔE_{def} of all fragments as the difference between their absolute deformation energy at scission and at full acceleration. Then, for each fragmentation the available excitation energy at scission can be obtained by subtracting the extra-deformation energies of complementary fragments from TXE. This available excitation energy at scission is shared between the complementary nascent fragments under the assumptions of a statistical equilibrium at scission (equal nuclear temperatures $\tau_L = \tau_H$) and level densities of nascent fragments in the Fermi-gas regime [14,15]. Consequently the available excitation energy at scission of each fragmentation E^*_{sc} is partitioned according to the ratio of the level density parameters of complementary nascent fragments, *i.e.*:

$$E^L_{sc}/E^H_{sc} = a^L_{sc}/a^H_{sc}$$
$$\text{and} \quad E^*_{sc} = TXE - (\Delta E^L_{def} + \Delta E^H_{def}) = E^L_{sc} + E^H_{sc}. \quad (1)$$

Note, for simplicity in eq. (1) as well as in other formulae referring to a fragment pair of the fragmentation range, the fragment specification (A,Z) is omitted. Finally the fragment excitation energy at full acceleration is obtained as a sum of the fragment excitation energy at scission resulting from eq. (1) and the extra-deformation energy:

$$E^*_{L,H} = E^{L,H}_{sc} + \Delta E^{L,H}_{def} \quad \text{with} \quad E^*_L + E^*_H = TXE. \quad (2)$$

Usually in the PbP treatment the energy-dependent level density parameters provided by the super-fluid model are used (see ref. [1] and references therein):

$$a(A,Z,E^*) = \begin{cases} \tilde{a}(A)\left(1 + \dfrac{\delta W(A,Z)}{U^*}[1-\exp(-\gamma(A)U^*)]\right), \\ \qquad U^* = E^* - E_{cond}, \quad E^* > E_{cr}, \\ a_{cr} = \tilde{a}(A)\left(1 + \dfrac{\delta W(A,Z)}{E_{cr}}[1-\exp(-\gamma(A)E_{cr})]\right), \\ \qquad E^* \le E_{cr}, \end{cases} \quad (3)$$

in which E^* is the excitation energy of the fragment and $\delta W(A,Z)$ is the shell correction. E_{cr} is the critical energy at which the phase transition between super-fluid and normal states occurs. The values of E_{cr} and a_{cr} are calculated iteratively using eq. (3) and $E_{cr} = a_{cr}t^2_{cr}$. The critical temperature is $t_{cr} = 0.567\Delta$ and the condensation energy is taken as $E_{cond} = 3a_{cr}\Delta^2/2\pi^2 - n\Delta$ where $\Delta = 12/\sqrt{A}$ is the pairing correlation function and $n = 0,1,2$ for even-even, odd-A and odd-odd nuclei, respectively. Different parameterizations of the damping of shell effects $\gamma(A) = \gamma_0 A^{-1/3}$ and the asymptotic value of the level density parameter $\tilde{a}(A) = \alpha A + \beta A^{2/3}$, *i.e.* different values of the parameters γ_0, α and β, can be used.

In the case of an energy-dependent level density parameter, *i.e.* eq. (3), the excitation energies at scission and the corresponding level density parameters of complementary nascent fragments are obtained simultaneously by an iterative procedure according to eq. (1). The level density parameters of fully accelerated fragments are obtained by applying eq. (3) in which E^* are the fragment excitation energies at full acceleration given by eq. (2).

Note, different other prescriptions for the level density parameter (*e.g.*, non-energy–dependent level density parameters, different systematics etc.) can be employed in the PbP model. The PbP results given in sect. 3 and the ones reported in a great part of previous papers (*e.g.* [1, 10–12]) were obtained with level density parameters of the super-fluid model, eq. (3).

As it was already mentioned in previous works (*e.g.*, refs. [1,9,14,15]) the excitation energy ratio at full acceleration E^*_H/TXE as a function of A_H exhibits a systematic behaviour with the following features: for fragment pairs with A_H less than $\sim$ 140–144 this ratio is less than 0.5 with a minimum placed at A_H around 130 (due to the magic or double magic heavy fragment with $N = 82$, $Z = 50$). The ratio E^*_H/TXE is of about 0.5 at A_H placed around 140 (which corresponds to the most probable fragmentation) and it exhibits an almost linear increase for A_H above this value. With increasing excitation energy the minimum value of this ratio at $\sim$ 130 is increasing.

The existing experimental data of prompt neutron multiplicity distribution $\nu(A)$ show the same systematic behaviour of the multiplicity ratio $\nu_H/(\nu_L + \nu_H)$ as a function of A_H. This behaviour was firstly mentioned by Wahl [8] and it was also discussed in detail in our previous papers (*e.g.*, refs. [9,15,16]).

2.3 Prompt emission corresponding to an individual fragment and fragmentation

The prompt neutrons are assumed to be emitted from fully accelerated fragments following a Weisskopf-Ewing statistical evaporation spectrum in the center-of-mass frame at a given residual fragment temperature T:

$$\varphi(\varepsilon) \propto \sigma_c(\varepsilon)\varepsilon \exp(-\varepsilon/T), \tag{4}$$

in which $\sigma_c(\varepsilon)$ is the compound nucleus cross-section of the inverse process of neutron evaporation from a fragment. The $\sigma_c(\varepsilon)$ of all fragments forming the fragmentation range are provided by optical model calculations using the code SCAT2 [17] with phenomenological potential parameterizations appropriate for nuclei appearing as fission fragments (usually of Becchetti-Greenless) taken from RIPL3 [18].

The sequential neutron emission is taken into account in a global way by a residual temperature distribution $P(T)$ leading to the following prompt neutron spectrum for an individual fragment in the center-of-mass frame:

$$\Phi(\varepsilon) = \sigma_c(\varepsilon)\varepsilon \int_0^{T_{\max}} k(T)P(T)\exp(-\varepsilon/T)\mathrm{d}T,$$
$$k(T) = \left(\int_0^{\infty} \sigma_c(\varepsilon)\varepsilon \exp(-\varepsilon/T)\mathrm{d}\varepsilon\right)^{-1}. \tag{5}$$

Different functions can be used for the residual temperature distribution $P(T)$, *e.g.* the triangular form proposed by Madland and Nix [5], the form proposed in ref. [19] or numerical residual temperature distributions obtained from the rigorous treatment of the sequential emission [20].

In the present work, as well as in other PbP calculations (*e.g.*, those reported in refs. [9,10,15]) the $P(T)$ form proposed by Madland and Nix [5], *i.e.*

$$P(T) = \begin{cases} \dfrac{2T}{T_m^2}, & T \le T_m, \\ 0, & T > T_m, \end{cases} \tag{6}$$

was used. This triangular form can approximate the sum of residual temperature distributions following the emission of each neutron resulting from the treatment of sequential emission [20]. $P(T)$ of eq. (6) is parameterized as a function of the temperature of initial fragments (before the first neutron is emitted) considered in the Fermi-gas regime of level density. Consequently the maximum temperature entering eq. (5) is T_m of eq. (6) given by

$$T_{mL,H} = \sqrt{E^*_{L,H}/a_{L,H}} \tag{7}$$

with the excitation energies $E^*_{L,H}$ and the level density parameters $a_{L,H}$ of fully accelerated fragments already calculated for all fragmentations as described in sect. 2.2.

The shape of the prompt neutron spectrum $\Phi(\varepsilon)$ of eq. (5) and of the average prompt neutron energy in the center-of-mass frame $\langle\varepsilon\rangle$ (*i.e.*, the first-order momentum of $\Phi(\varepsilon)$) are influenced by the shape of the compound nucleus cross-section $\sigma_c(\varepsilon)$, driven by different optical model parameterizations.

The prompt neutron spectrum in the laboratory frame corresponding to a fragment of the fragmentation range is calculated as

$$N(E) = \int_{(\sqrt{E}-\sqrt{E_f})^2}^{(\sqrt{E}+\sqrt{E_f})^2} \frac{\Phi(\varepsilon)}{4\sqrt{\varepsilon E_f}}\mathrm{d}\varepsilon, \tag{8}$$

in which $\Phi(\varepsilon)$ is given by eq. (5), E is the neutron energy in the laboratory frame and E_f is the average kinetic energy per nucleon obtained from momentum conservation for each pair of fragments forming the fragmentation range, *i.e.* $E_{fL,H} = (A_{H,L}/A_{L,H})(TKE/(A_L + A_H))$.

Obviously the shape of the prompt neutron spectrum in the laboratory frame is also influenced by the shape of $\sigma_c(\varepsilon)$ driven by different optical model parameterizations and it is influenced by the form of $P(T)$, too.

Note, the PbP results of this paper as well as the majority of PbP results previously reported were obtained by using $\sigma_c(\varepsilon)$ from optical model calculations with the Becchetti-Greenlees potential and the $P(T)$ form of eq. (6).

It is known that the most important emission of prompt neutrons takes place at the full acceleration of fragments. But neutron evaporation during fragment acceleration can be possible, too, leading to a non-isotropic neutron spectrum in the center-of-mass frame. Terrel [21] assumed that the anisotropy of neutron emission, if present, is symmetrical about 90°, *i.e.* $\Phi(\varepsilon,\theta_{cm}) = \Phi(\varepsilon)(1+b\cos^2\theta_{cm})/(1+b/3)$, where $\Phi(\varepsilon)$ is given by eq. (5) and b is the anisotropy parameter. By replacing $\cos\theta_{cm}$ from $E = \varepsilon + E_f + 2\sqrt{\varepsilon E_f}\cos\theta_{cm}$ in the expression of $\Phi(\varepsilon,\theta_{cm})$, the prompt neutron spectrum in the laboratory frame becomes

$$N(E) = \int_{(\sqrt{E}-\sqrt{E_f})^2}^{(\sqrt{E}+\sqrt{E_f})^2} \frac{\Phi(\varepsilon)}{4\sqrt{\varepsilon E_f}} \frac{1+b(E-\varepsilon-E_f)^2/4\varepsilon E_f}{1+b/3}\mathrm{d}\varepsilon. \tag{9}$$

Note, in the majority of PbP calculations the anisotropy is not taken into account, *i.e.* $b = 0$, the spectrum being expressed by eq. (8), because of the difficulty to assign values of the anisotropy parameter for each fragment. Furthermore, in the majority of cases, the prompt neutron spectrum results have described well the experimental data without including anisotropy.

In the case of the most probable fragmentation approach, *i.e.* the LA model of Madland and Nix [5] and Madland and Kahler [6], when the model parameters are average values, the value assigned to the anisotropy parameter is also an average one. The same situation, *i.e.* an average value of b, is in the case of the multi-modal fission treatment when a most probable fragmentation (with average model parameters) is considered for each fission mode, *e.g.* ref. [19].

In the case of prompt emission quantities referring to a fragment pair, the excitation energy ratio $E^*_H/TXE(A_H)$ (with the systematic behaviour mentioned in sect. 2.2)

can be used to express the weight of the complementary fragments, *i.e.*

$$r_H = E_H^*/TXE, \qquad r_L = 1 - r_H = E_L^*/TXE. \quad (10)$$

For instance the average prompt neutron energy in the center-of-mass frame corresponding to a fragment pair is $\langle\varepsilon\rangle_{pair} = r_L\langle\varepsilon_L\rangle + r_H\langle\varepsilon_H\rangle$ (in which $\langle\varepsilon_L\rangle$ and $\langle\varepsilon_H\rangle$ are the first-order momenta of the prompt neutron spectrum of eq. (5)), the prompt neutron spectra of a fragmentation in the center-of-mass and laboratory frames are $\Phi_{pair}(\varepsilon) = r_L\Phi_L(\varepsilon)+r_H\Phi_H(\varepsilon)$ and $N_{pair}(E) = r_L N_L(E)+r_H N_H(E)$, respectively (with $\Phi_{L,H}(\varepsilon)$ given by eq. (5) and $N_{L,H}(E)$ given by eqs. (8) or (9)).

Different prompt emission quantities corresponding to each fission fragment can be calculated, too. As examples, the energy carried away per neutron, which is expressed as

$$\eta = \langle\varepsilon\rangle + \langle S_n\rangle \quad (11)$$

and the average prompt γ-ray energy:

$$\langle E_\gamma\rangle = E^* - \nu\eta. \quad (12)$$

The average neutron separation energy of each fragment $\langle S_n\rangle$, entering eq. (11), is calculated by an iterative procedure accounting for sequential emission [1,9,20]. If the excitation energy of a fully accelerated initial fragment $E^*(A,Z)$ exceeds its neutron separation energy $S_n(A,Z)$ a neutron can be emitted (in competition with γ emission). If the excitation energy of the first residual fragment exceeds its neutron separation energy $S_n(A-1,Z)$, a second neutron can be evaporated etc. A total number of k neutrons can be emitted when the excitation energy of the k-th residual nucleus is less than $S_n(A-k,Z)$. The average neutron separation energy corresponding to an individual initial fragment is then $\langle S_n\rangle(A,Z) = \frac{1}{k}\sum_{i=0}^{k-1} S_n(A-i,Z) = S_{kn}(A,Z)/k$. The values of $S_n(A-i,Z)$ are obtained using the mass excesses from nuclear data libraries (*e.g.*, Audi and Wapstra from RIPL3 [13]). E^* entering eq. (12) is the fragment excitation energy at full acceleration resulting from the TXE partition given by eq. (2), η is the energy carried away per neutron of eq. (11) and ν is the prompt neutron multiplicity of the respective fragment. The prompt neutron multiplicity corresponding to each fragmentation (pair of fragments at a given TKE) is $\nu_{pair} = r_L\nu_L + r_H\nu_H$, in which r_L and r_H are the weights of complementary fragments given by eq. (10).

The prompt fission energy deposition in the medium is defined for a fragment pair according to ref. [22]:

$$E_{d\,pair} = Q + B_n + E_n - \nu_{pair}\langle S_n\rangle_{pair} \quad (13)$$

with the Q-value based on mass excesses as mentioned at the beginning of sect. 2.2 and the average neutron separation energy of a fragment pair $\langle S_n\rangle_{pair}$ based on the weights of complementary fragments. In the case of spontaneous fission both B_n and E_n are zero in eq. (13). Using the energy conservation for a fragment pair, the prompt fission energy deposition in the medium corresponding to an individual fragment at a given TKE can be also obtained as

$$E_d = E_k + \nu\langle\varepsilon\rangle + E_\gamma \quad (14)$$

in which E_k is the fragment kinetic energy deduced from momentum conservation for each TKE value of the fragmentation range: $E_k^{L,H} = TKEA_{H,L}/(A_L + A_H)$.

Note, if for some fragmentations at some TKE values, one of the complementary fragments has an excitation energy value (resulting from the TXE partition) that is less than the neutron separation energy of the respective fragment, then the prompt neutron multiplicity, the spectrum and other prompt emission quantities of the respective pair are those of the fragment able to emit neutrons. If the excitation energies of both fragments are less than their neutron separation energies the respective fragmentation is eliminated from calculations.

2.4 Multi-parametric matrices

All prompt emission quantities described in sect. 2.3 and the fragment properties described in sect. 2.2 are multi-parametric matrices, *i.e.* they are functions of fragment (denoted as (A,Z)) or of fragment pair (denoted (A_L,Z_L,A_H,Z_H) or (A,Z,A_0-A,Z_0-Z)) and of TKE. *E.g.*, the fragment level density parameter $a(A,Z,TKE)$, the fragment excitation energy at full acceleration $E^*(A,Z,TKE)$, the fragment average neutron separation energy $\langle S_n\rangle(A,Z,TKE)$, the prompt neutron multiplicity $\nu(A,Z,TKE)$ and so on. As in other works, these multi-parametric matrices are generically labeled as $q(A,Z,TKE)$.

These multi-parametric matrices are considered as primary results of the PbP model because they do not depend on the fragment distribution $Y(A,Z,TKE)$. The calculation of these matrices needs only data from nuclear data libraries, *e.g.* mass excesses, shell corrections, β_2 deformation parameters, optical model parameterizations adequate for nuclei appearing as fission fragments, different parameterizations corresponding to the level density prescription used, etc., all these data being included in the databases of RIPL1-3 of the IAEA.

The most important validation of any prompt emission model, hence of the PbP model too, is to compare the multi-parametric matrices of different quantities with existing experimental data. This can be considered as a validation of the model itself because the multi-parametric matrices do not depend on fragment distributions.

The recent measurement of the prompt neutron multiplicity matrix $\nu(A,TKE)$ of the fissioning nucleus ^{252}Cf(SF) performed by Göök and co-workers [2] offers this possibility.

Older data of Nifenecker *et al.* [23] referring to the E_γ matrix of ^{252}Cf(SF) as well as the experimental multiplicity matrices of ^{252}Cf(SF) (data of Zackharova and of Bowman) and of ^{233,235}U(n_{th},f) measured by Nishio were already used to validate the primary results of the PbP model, see refs. [1,24] and references therein.

Note, the existing experimental matrices refer to prompt emission quantities as a function only of fragment mass A and of TKE. Consequently, the PbP multi-parametric matrices $q(A, Z, TKE)$ are averaged over Z, *i.e.* over the isobaric charge distribution (mentioned in sect. 2.1).

2.5 Average prompt emission quantities

A second step of the validation of prompt emission models consists in the comparison of model results with existing experimental data referring to average quantities as a function of fragment mass or as a function of TKE and with the data of total average quantities (*i.e.* not depending on fragment and TKE).

Consequently, the agreement with these data depends not only on the PbP model itself but also on the reliability of the fragment distribution $Y(A, Z, TKE)$ on which the PbP multi-parametric matrices are averaged.

Different average quantities $\overline{q}(A)$, $\langle q\rangle(TKE)$, $\langle q\rangle_{tot}$ which can be compared with existing experimental data are obtained as

$$\bar{q}(A) = \sum_{Z,TKE} q(A,Z,TKE)Y(A,Z,TKE) \Big/ \sum_{Z,TKE} Y(A,Z,TKE), \tag{15a}$$

$$\langle q\rangle(TKE) = \sum_{A,Z} q(A,Z,TKE)Y(A,Z,TKE) \Big/ \sum_{A,Z} Y(A,Z,TKE), \tag{15b}$$

$$\langle q\rangle_{tot} = \sum_{A,Z,TKE} q(A,Z,TKE)Y(A,Z,TKE) \Big/ \sum_{A,Z,TKE} Y(A,Z,TKE), \tag{15c}$$

where the multi-parametric distribution $Y(A, Z, TKE) = p(Z, A)Y_{\exp}(A, TKE)$ (in which $p(Z, A)$ is the Gaussian isobaric charge distribution mentioned in sect. 2.1) includes the experimental distribution $Y_{\exp}(A, TKE)$. In the present work the experimental two-dimensional distribution $Y(A, TKE)$ of ^{252}Cf(SF) measured by Göök *et al.* [2] and the one of ^{235}U(n_{th}, f) measured by Al-Adili *et al.* [4] were used.

The prompt neutron multiplicity distribution $P(\nu)$ deserves a mention, too, because $P(\nu)$ is extremely sensitive to both, the prompt neutron multiplicity matrix $\nu(A, Z, TKE)$ and the fragment distribution $Y(A, Z, TKE)$. $P(\nu)$ is a histogram obtained by counting in the matrix $\nu(A, Z, TKE)$ the probability to have the prompt neutron multiplicity value between 0 and 1, 1 and 2, 2 and 3, etc. This probability is the sum of the probabilities of the fragment A, Z with the total kinetic energy TKE (*i.e.*, the $Y(A, Z, TKE)$ value) which emits the respective number of neutrons. Improved $P(\nu)$ results compared to the previous results reported in 2010 [25] are given in sect. 3.

2.6 Los Alamos model parameters provided by the PbP treatment

During the time the PbP treatment has provided input parameters of the classical LA model of Madland and Nix [5] (with equal T_m), *i.e.* $\langle E_r\rangle$ (energy release), $\langle TKE\rangle$, $\langle S_n\rangle$ and $\langle C\rangle = A_0/\langle a\rangle$ (A_0 the mass number of the fissioning nucleus). These parameters are total average values calculated according to eq. (15c) in which the following multi-parametric matrices are used: the Q-values for the energy release, $\langle S_n\rangle(A, Z, TKE)$, $a(A, Z, TKE)$ (eq. (3) applied at full acceleration, *i.e.* at E^* resulting from the TXE partition by modeling at scission). For $\langle TKE\rangle$ existing experimental data were used. This PbP treatment was the basis of the systematic of the LA model parameters elaborated in 2009 [7].

In the LA model of Madland and Nix [5] the same $P(T)$ distribution with the triangular form given by eq. (6), *i.e.* the same T_m value, was considered for both fragments of the so-called most probable fragmentation. This is an equivalent value of T_m calculated as $T_m = \sqrt{\langle TXE\rangle/\langle a\rangle}$. In ref. [5] the total average level density parameter $\langle a\rangle$ is expressed by the parameter $\langle C\rangle = A_0/\langle a\rangle$. As we have already reported (*e.g.*, refs. [1,9,16] and references therein) for many fissioning nuclei the use of the super-fluid model with the parameterization of Ignayiuk [26] leads to average level density parameter values giving an average C-parameter of about 11 MeV, as mentioned by Madland and Nix [5]. Other details about the equivalent T_m and the C-parameter can be found in ref. [16].

Note, in the total prompt neutron spectrum expression of the LA model of Madland and Nix [5] the consideration of equal weights of complementary fragments ($r_L = r_H = 1/2$) can be also justified by taking into account that at A_H around 140, which corresponds to the most probable fragmentation, the existing experimental $\nu(A)$ data show an almost equal number of neutrons emitted by the complementary fragments (see the systematic behaviour of $\nu_H/(\nu_L + \nu_H)$ and of E^*_H/TXE as a function of A_H mentioned in sect. 2.2).

A refined Los Alamos model was recently reported by Madland and Kahler in ref. [6]. The improvement consists in the use of non-equal T_m (entering $P(T)$ of eq. (6)) for the light and heavy fragments of the most probable fragmentation, as it is considered in the PbP treatment for each pair of fragments of the fragmentation range, see eq. (7).

The values of the input parameters of this improved LA model of Madland and Kahler, *i.e.* $\langle E^*_L\rangle$, $\langle E^*_H\rangle$, $\langle a_L\rangle$, $\langle a_H\rangle$, $\langle S^L_n\rangle$, $\langle S^H_n\rangle$, $\langle E^L_\gamma\rangle$, $\langle E^H_\gamma\rangle$ can also be obtained from the PbP treatment by averaging the corresponding multi-parametric matrices (described in sects. 2.2, 2.3 and 2.4) as in eq. (15c) but this time separately for the light and heavy fragment groups. The values of the non-equal T_m are then obtained as $T^{L,H}_m = \sqrt{\langle E^*_{L,H}\rangle/\langle a_{L,H}\rangle}$.

Comparisons of prompt fission neutron spectra provided by the improved LA model of Madland and Kahler [6] with the input parameters resulting from the PbP treatment and the parameters from ref. [6] are given in sect. 3.

3 PbP model results in comparison with the experimental data of ^{252}Cf(SF) and ^{235}U(n_{th}, f)

Indubitably ^{252}Cf(SF) is the fissioning nucleus benefiting of the most numerous experimental data for fragments and prompt emission, being considered as the standard nucleus for prompt emission in fission. On the second place regarding the prompt fission data is the standard neutron-induced reaction ^{235}U(n_{th}, f).

In the present work a detailed comparison of the PbP model results with all available data is performed just for these two fissioning systems. Results of the PbP model for both ^{252}Cf(SF) and ^{235}U(n_{th}, f) were already reported in our previous papers (*e.g.*, refs. [1,9–12,14,15,25] and references therein) where they were compared with experimental data existing at that time or were referring only to a part of prompt emission quantities in connection with the subjects of the respective papers.

The new experimental data for ^{252}Cf(SF) of Göök *et al.* [2] concerning both the prompt neutron multiplicity matrix $\nu(A, TKE)$ and the fission fragment distribution $Y(A, TKE)$ are more accurate and complete than the previous literature data. They offer the possibility not only of a more detailed validation of the PbP model as previously but also of a more consistent validation because the same experimental $Y(A, TKE)$ distribution of Göök is used in the averaging of the PbP multi-parametric matrices.

In the case of ^{235}U(n_{th}, f) we present PbP results compared especially with the very recent experimental data of Göök and co-workers reported in ref. [3]. These data have become available after the PbP calculation performed in this work. The good agreement of these data with the PbP results confirms the PbP model prediction for the prompt emission quantities $\langle\nu\rangle(TKE)$ and $\langle\varepsilon\rangle(A)$ of ^{235}U(n_{th}, f).

The PbP results are organized in subsections reflecting the type of prompt emission quantity, *i.e.* multi-parametric matrices $q(A, TKE)$, average quantities as a function of A, $\overline{q}(A)$, average quantities as a function of TKE, $\langle q\rangle(TKE)$ and the $P(\nu)$ distribution. Total average values of different prompt emission quantities, $\langle q\rangle_{tot}$, are also mentioned. Results of the total prompt neutron spectrum including comparisons with the new version of the LA model are exemplified, too.

In the present PbP calculations the fragmentation range was constructed by taking 3 charge numbers Z at each A and using the charge polarizations $\Delta Z(A)$ and the $rms(A)$ of the isobaric charge distributions of Wahl [8]. The TKE range was taken from 140 to 215 MeV for ^{252}Cf(SF) and from 100 to 195 MeV for ^{235}U(n_{th}, f), in both cases with a step of 5 MeV.

The PbP results given in this section were obtained by using fragment level density parameters (at scission and at full acceleration) provided by the super-fluid expression of eq. (3) with the shell corrections of Möller and Nix from RIPL3 [27] and the γ and $\tilde{a}$ parameterizations of Ignatiuk [26]. The optical model calculations of $\sigma_c(\varepsilon)$ were done with the parameterization of Becchetti-Greenlees [18].

3.1 Matrices of prompt emission quantities

The most relevant validation of the PbP model is the comparison of the prompt neutron multiplicity matrix $\nu(A, TKE)$ with the experimental $\nu(A, TKE)$ data of ^{252}Cf(SF) measured by Göök *et al.* [2].

Note, the experimental $\nu(A, TKE)$ data of ref. [2] were normalized to the standard value $\langle\nu\rangle_{tot} = 3.759$ from the Evaluated Nuclear Data Library ENDF [28].

Figures 1–3 show the dependence on TKE of the average prompt neutron multiplicity per fragment mass as well as of the mass pair, for mass numbers covering the entire range of the experiment of Göök *et al.* [2] (with A_L and A_H, indicated in each frame). The experimental data of Göök *et al.* are plotted with full gray squares for the heavy fragment (ν_H), open black circles for the light fragment (ν_L) and full black diamonds for the pair (ν_{pair}). The PbP results are given with small circles connected with solid lines colored in blue (ν_H), green (ν_L) and red (ν_{pair}).

As can be seen the PbP results describe very well the experimental data.

Note, at low TKE values, below 160 MeV, the experimental data deviate from the linear trend (especially for heavy fragment masses $A_H \sim 130$ for which the prompt neutron multiplicity is very low). These deviations are not considered important due to the low statistical significance.

Figure 4 shows the dependence on mass of the average prompt neutron multiplicity per fragment (right part) and fragment pair (left part) at TKE values ranging from 160 MeV to 195 MeV. The data of Göök *et al.* are plotted with full squares and the PbP results with open circles connected with solid lines. The experimental data are well described by the PbP results. In the right part of fig. 4 it can be also seen that $\nu(A)$ at a given TKE value exhibit a sawtooth shape.

Experimental data of prompt γ-ray energy of fragment mass pairs as a function of TKE for ^{252}Cf(SF) were reported by Nifenecker *et al.* [23]. These data plotted with open squares in fig. 5 are very well described by the PbP results (full blue circles connected with solid lines). The almost linear decrease of E_γ with increasing TKE is visible for all fragment mass pairs.

In the case of ^{235}U(n_{th}, f) the comparison of the $\nu(A, TKE)$ matrix with the data of Nishio was already reported in refs. [24,29].

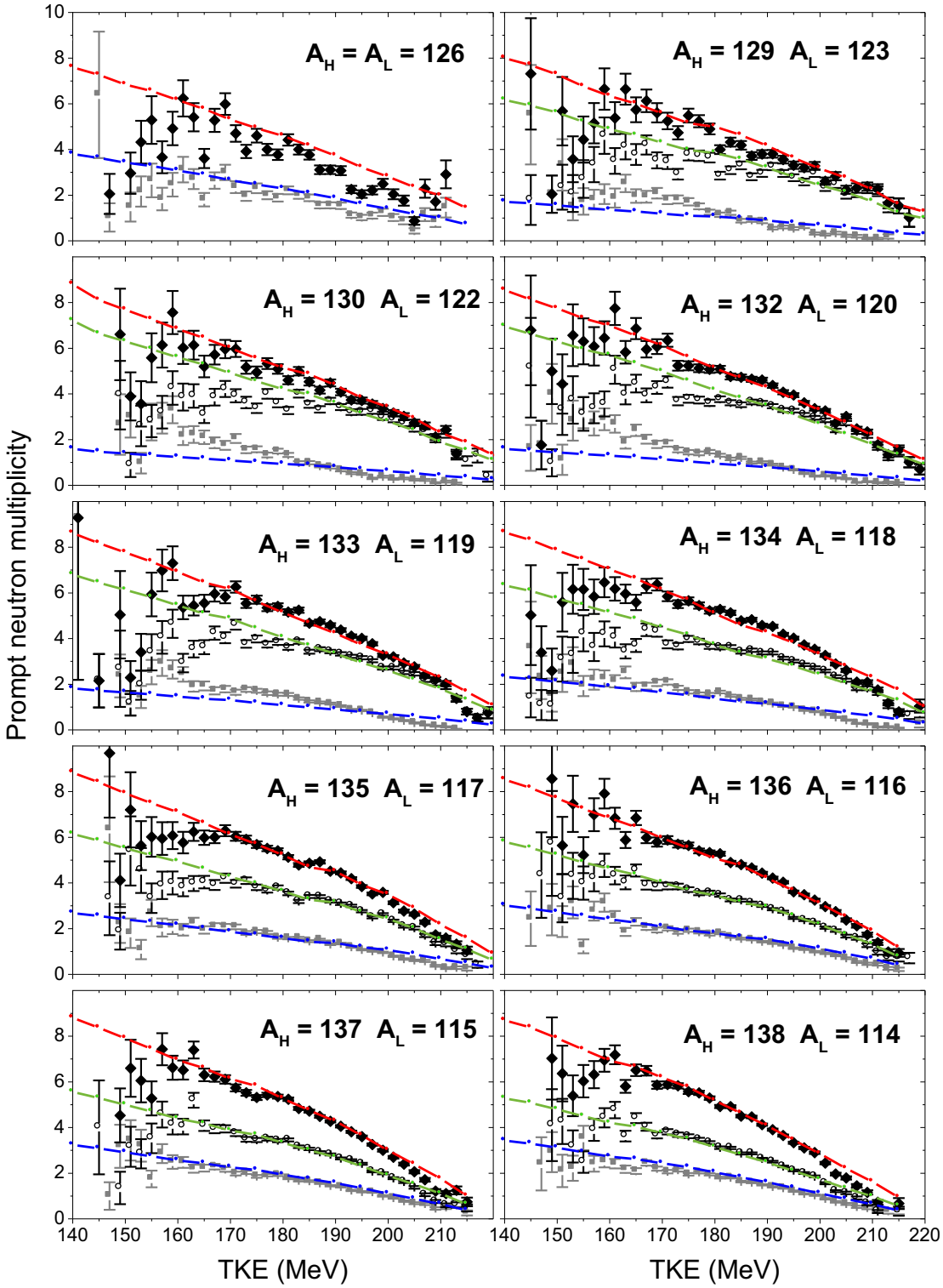

Fig. 1. $\nu_L(TKE)$, $\nu_H(TKE)$ and $\nu_{pair}(TKE)$ of ^{252}Cf(SF) for ten mass pairs with A_H ranging from 126 to 138. The experimental data of Göök *et al.* [2] are plotted with open black circles for $\nu_L(TKE)$, full gray squares for $\nu_H(TKE)$ and full black diamonds for $\nu_{pair}(TKE)$. The PbP results are plotted with small full circles connected with lines colored in green (ν_L), blue (ν_H) and red (ν_{pair}).

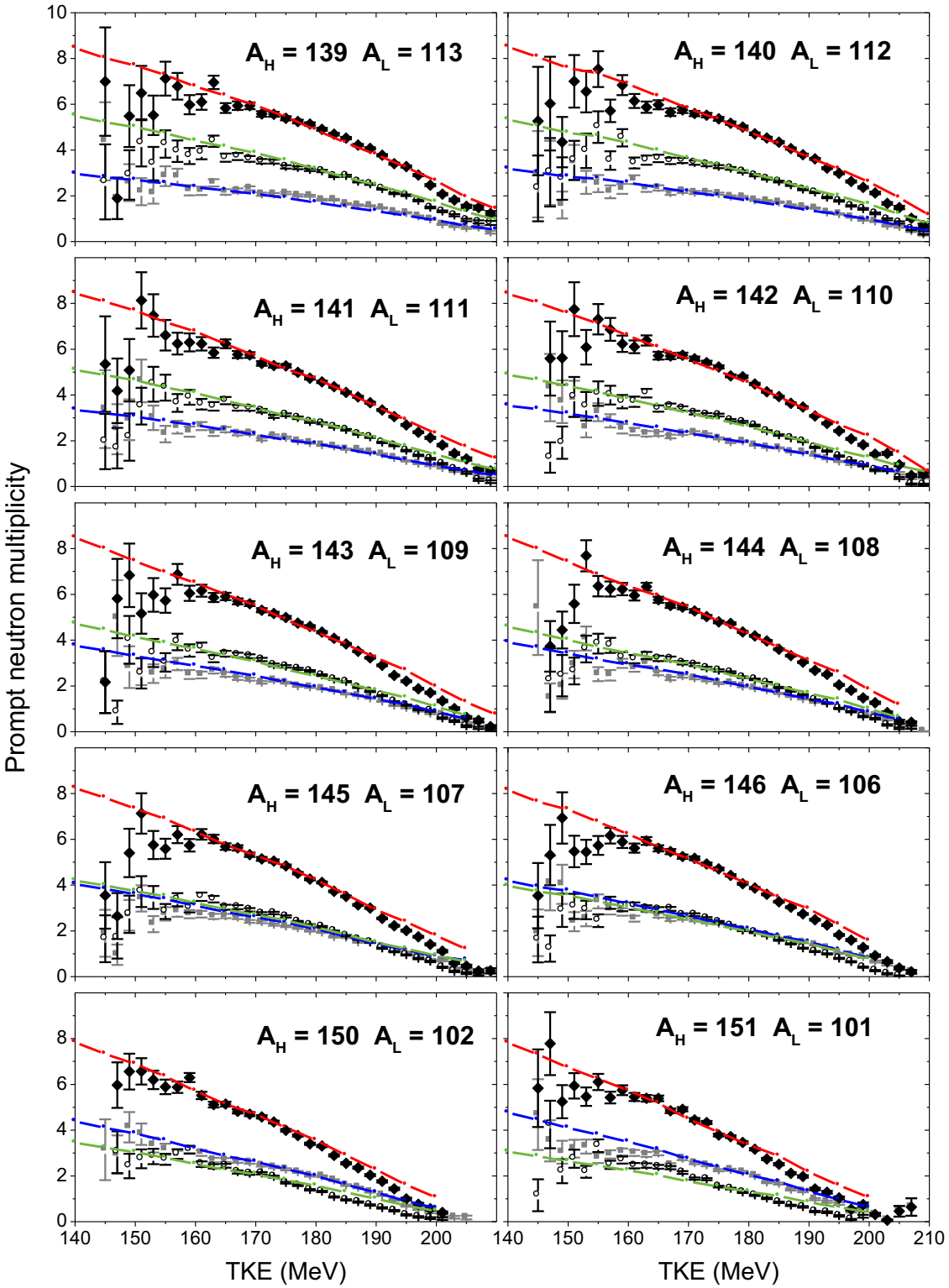

Fig. 2. $\nu_L(TKE)$, $\nu_H(TKE)$ and $\nu_{pair}(TKE)$ of ^{252}Cf(SF) for ten mass pairs with A_H ranging from 139 to 151. The experimental data of Göök *et al.* [2] are plotted with open black circles for $\nu_L(TKE)$, full gray squares for $\nu_H(TKE)$ and full black diamonds for $\nu_{pair}(TKE)$. The PbP results are plotted with small full circles connected with lines colored in green (ν_L), blue (ν_H) and red (ν_{pair}).

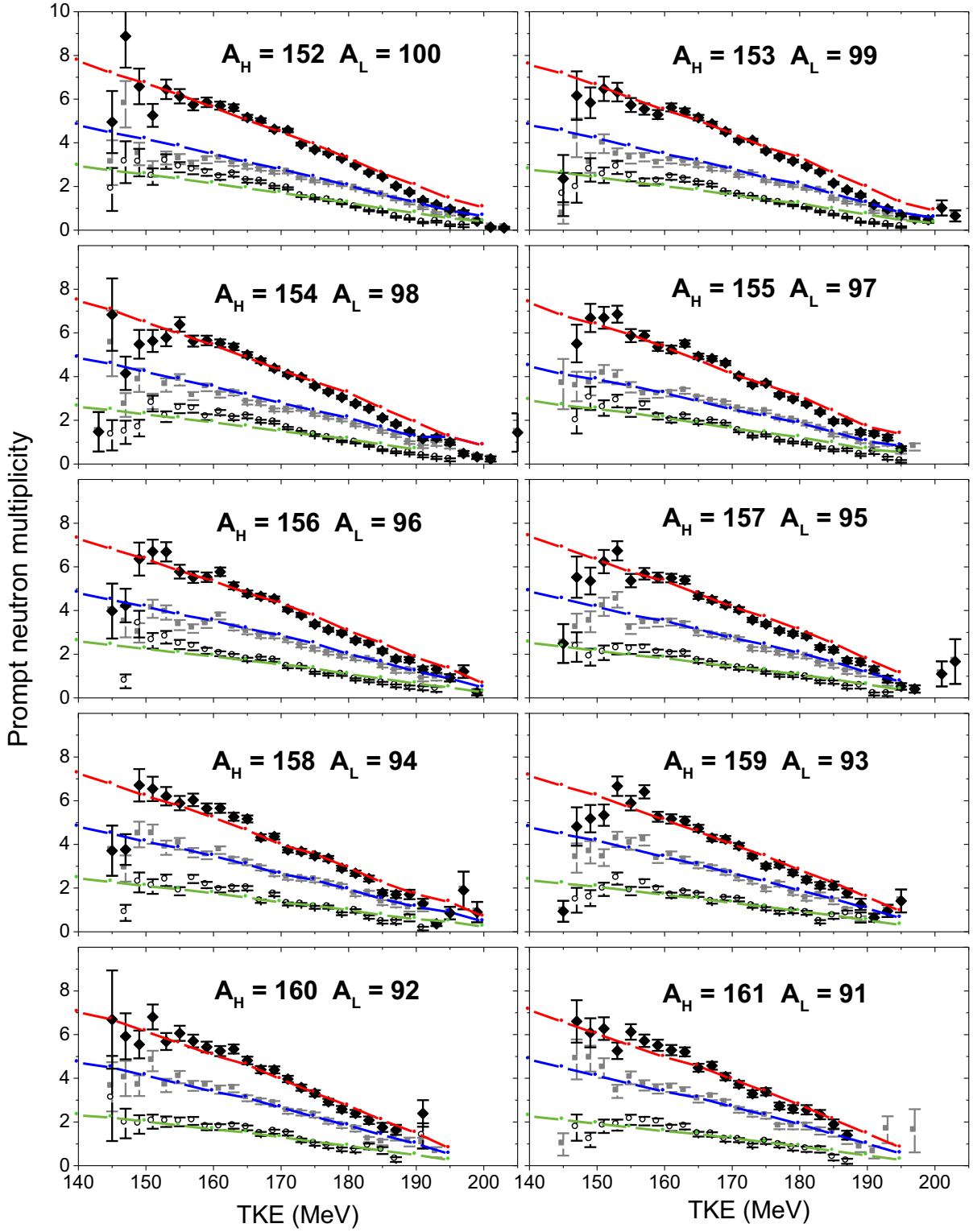

Fig. 3. $\nu_L(TKE)$, $\nu_H(TKE)$ and $\nu_{pair}(TKE)$ of ^{252}Cf(SF) for ten mass pairs with A_H ranging from 152 to 161. The experimental data of Göök *et al.* [2] are plotted with open black circles for $\nu_L(TKE)$, full gray squares for $\nu_H(TKE)$ and full black diamonds for $\nu_{pair}(TKE)$. The PbP results are plotted with small full circles connected with lines colored in green (ν_L), blue (ν_H) and red (ν_{pair}).

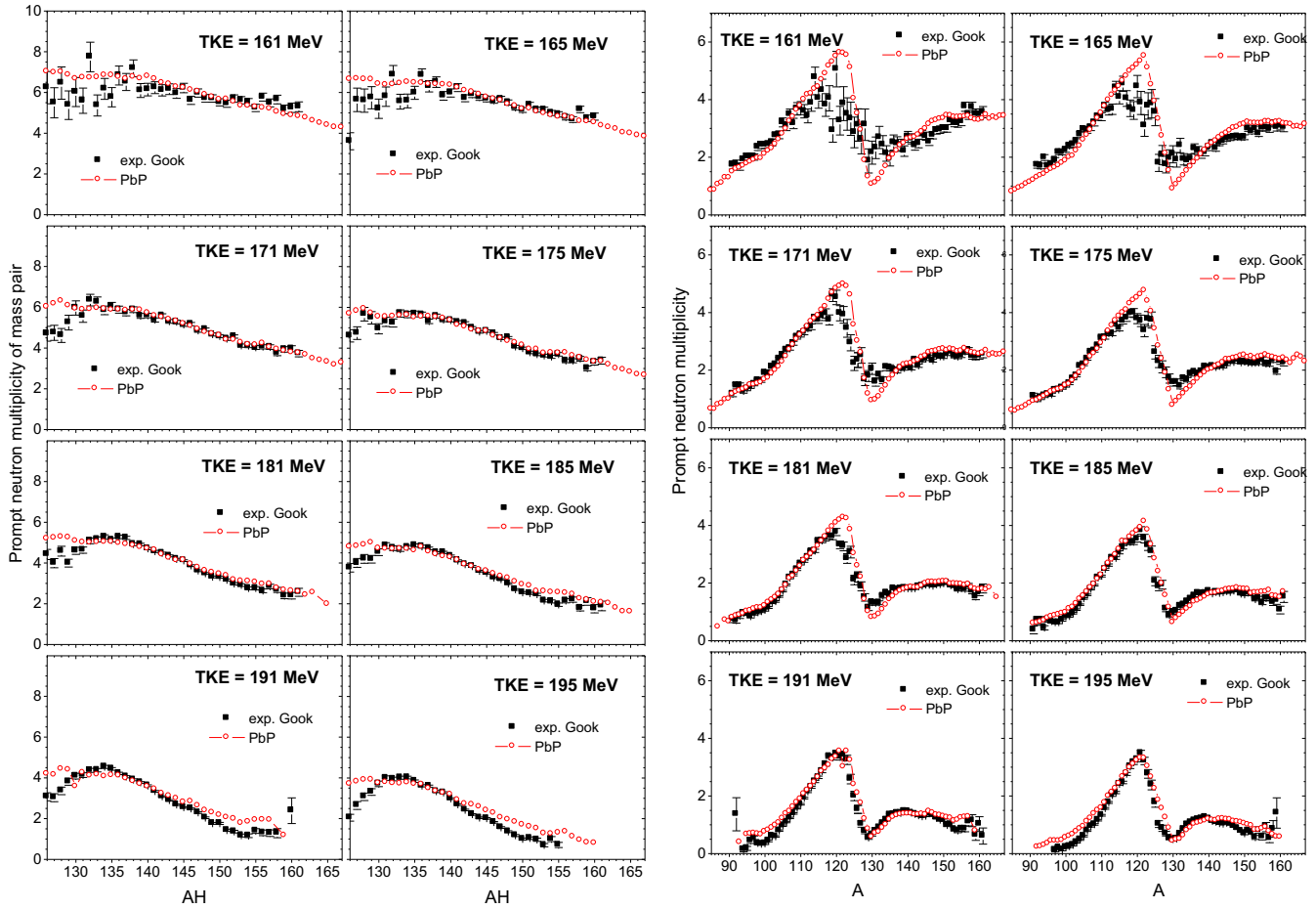

Fig. 4. $\nu_{pair}(A_H)$ (left part) and $\nu(A)$ (right part) of ^{252}Cf(SF) at a given TKE value (indicated in each panel). The experimental data of Göök *et al.* [2] are plotted with full black squares and the PbP results with open red circles.

3.2 Average quantities as a function of fragment mass A

Different average quantities as a function of fragment mass A, obtained according to eq. (15a), are compared with the existing experimental data and/or other model calculations as follows.

The most relevant quantity is the prompt neutron multiplicity as a function of A, $\nu(A)$, which is very sensitive to the TXE partition. On the contrary, the prompt neutron multiplicity of a fragment pair has a very low sensitivity to the energy partition, see ref. [9] for details.

Figure 6 shows prompt neutron multiplicity results as a function of A for ^{252}Cf(SF) in comparison with the existing experimental data, including the recent data of Göök *et al.* [2] (plotted with full black diamonds). As can be seen in the upper part the PbP result of $\nu(A)$ (full red circles) is in good agreement with all data sets (different black and gray symbols). The data of Budtz-Jorgensen and Knitter [30] (full gray squares) are very well described over the entire A range except for $A < 100$. The data of Göök *et al.* [2] (full black diamonds) are well described, too. Because the $\nu(A)$ distribution is the most sensitive quantity to the TXE partition, the good agreement of the $\nu(A)$ result with the experimental data validates the TXE partition method of PbP based on modeling at scission (mentioned in sect. 2.2 and discussed in detail in ref. [15] and references therein).

The present result of the ratio ν_H/ν_{pair} as a function of A_H (red circles in the lower part of fig. 6) is in good agreement with the data of Göök *et al.* (full black squares) and with the other data sets, too (different black and gray symbols). The excitation energy ratio E^*_H/TXE resulting from modeling at scission [14,15] (green stars) and the linear parameterization discussed in ref. [16] (blue line) are also given for comparison. The good description of the systematic behaviour of the ratio $\nu_H/\nu_{pair}(A_H)$ is an important validation, too.

Prompt neutron multiplicity results of ^{235}U(n_{th}, f), *i.e.* $\nu(A)$, $\nu_{pair}(A)$ and especially the systematic behaviour of the multiplicity ratio ν_H/ν_{pair} as a function of A_H were already reported, *e.g.* in ref. [9] (related to the sensitivity of prompt neutron multiplicity to different model prescriptions and $Y(A, TKE)$ distributions) and ref. [15] (related to TXE partition methods based on modeling at scission). In these papers the prompt neutron multiplicity results were compared with the experimental data available at that time in the EXFOR library and literature.

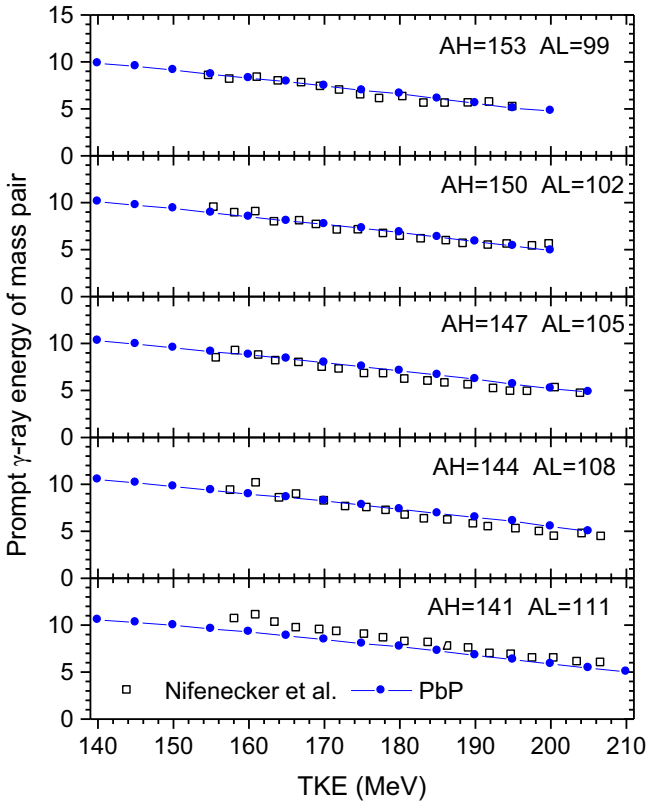

Fig. 5. ^{252}Cf(SF): Average prompt γ-ray energy as a function of TKE for a given fragment mass pair (with A_L and A_H indicated in each panel). The data of Nifenecker *et al.* are plotted with open squares and the PbP results with blue circles connected with solid lines.

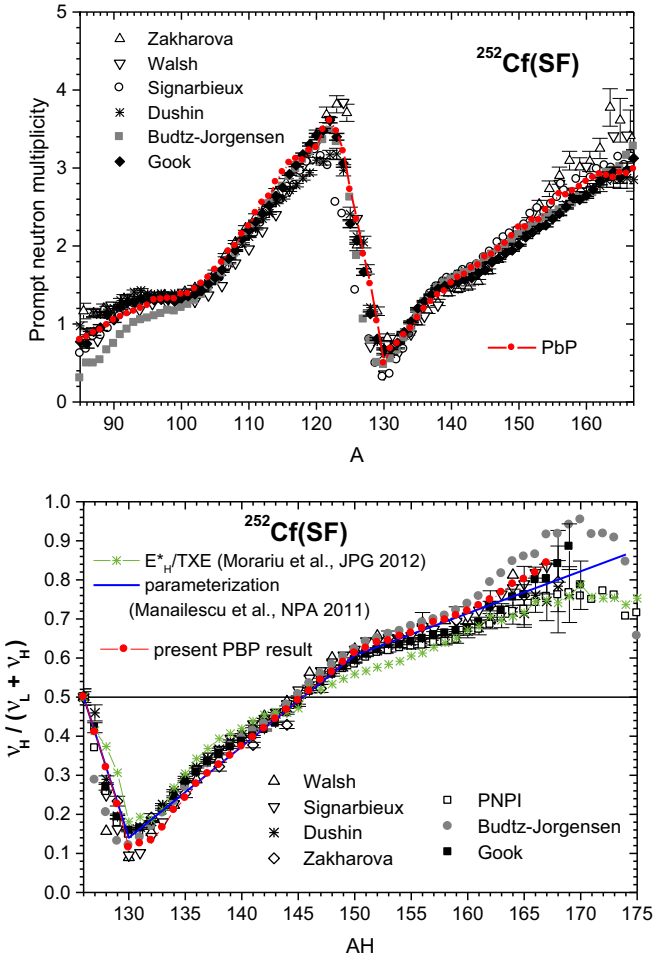

Fig. 6. Upper part: present result of $\nu(A)$ (red circles) in comparison with the experimental data (different black and gray symbols). Lower part: the ratio $\nu_H/\nu_{pair}(A_H)$; the experimental data (different black and gray symbols), the present PbP result (red circles), the linear parameterization of ref. [16] (blue line) and the E^*_H/TXE result based on the modeling at scission described in ref. [14] (green stars).

Prompt neutron multiplicity of ^{235}U(n, f) in the incident energy region of resolved resonances was recently measured at the GELINA facility of JRC-Geel. These data, reported by Göök *et al.* [3] as an average over the incident neutron energy range 0.3 eV–4.5 keV, are included in the present comparison. They are plotted with full black squares in fig. 7.

The data of Göök *et al.* [3] show an overall good agreement with the data of earlier experiments performed at thermal incident neutron energy (different gray and open black symbols). However, as can be seen in the upper part of fig. 7, the minima around $A \sim 80$ for the light fragments and ~ 130 for the heavy fragments appear more pronounced in the recent data of ref. [3].

The present PbP results of $\nu(A)$ and $\nu_{pair}(A)$, plotted with red circles, are close to the previous PbP results of ref. [14] (given with blue stars) which were obtained by taking only 2 charge numbers Z per A in the fragmentation range and by averaging over the distribution of ref. [31].

The PbP results of $\nu(A)$ (upper part of fig. 7) describe well the ensemble of experimental data over the entire mass range (except the region near symmetric fission where the experimental data scatter a lot due to the very low yield).

As can be seen in the lower part of fig. 7, the present $\nu_{pair}(A)$ result (full red circles) describes very well the recent data of Göök *et al.* [3] in the asymmetric fission region, *i.e.* at A_H above 125.

Note, the present PbP calculation, including $\nu(A)$, was performed before the experimental $\nu(A)$ data of Göök *et al.* [3] became available.

The average prompt neutron energy in the center-of-mass frame of ^{252}Cf(SF) $\langle\varepsilon\rangle$ as a function of A were measured by Budtz-Jorgensen and Knitter [30] and recently by Göök *et al.* [2]. These two data sets (being in good agreement) are plotted in fig. 8 with open diamonds and open squares, respectively, together with the result of the FIFRELIN code reported by Litaize *et al.* [32] (green stars). The PbP result is plotted with full red circles. The FIFRELIN and PbP results are in reasonable agreement and both describe the experimental data in the asymmetric fission region. Differences between the experimental

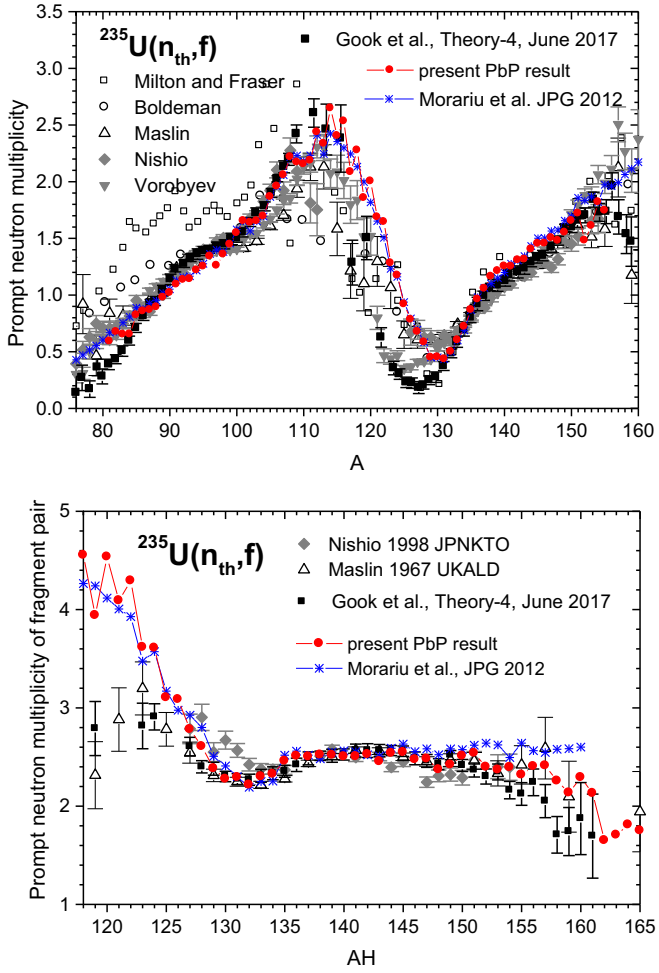

Fig. 7. $\nu(A)$ (upper part) and $\nu_{pair}(A_H)$ (lower part) of ^{235}U(n_{th}, f): the present PbP result (red circles) and the previous result reported in ref. [14] (blue stars) in comparison with earlier experimental data measured at thermal incident energy (different gray and open black symbols) and the very recent data of Göök *et al.* [3] (black squares).

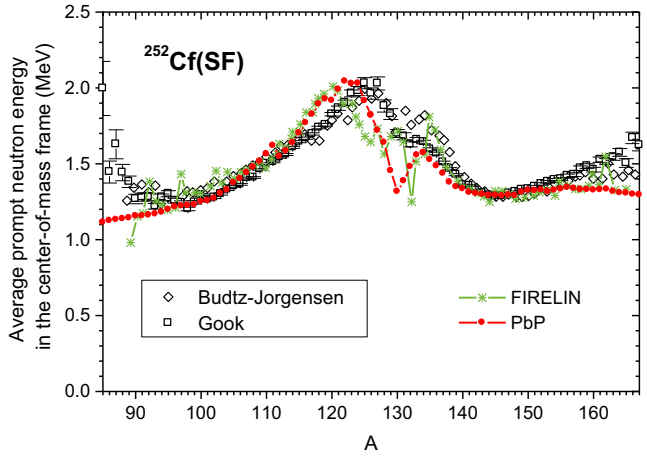

Fig. 8. $\langle\varepsilon\rangle(A)$ of ^{252}Cf(SF): the experimental data of Budtz-Jorgensen and Knitter (open black diamonds) and of Göök *et al.* (open black squares) and the results of FIFRELIN (green stars) and PbP (red circles).

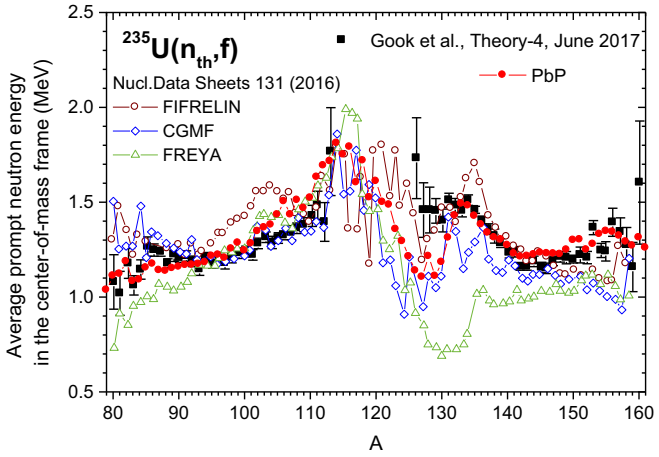

Fig. 9. The PbP results of $\langle\varepsilon\rangle(A)$ of ^{235}U(n_{th}, f) (full red circles) in comparison with the results of three Monte Carlo codes reported in ref. [1], *i.e.* FIFRELIN (open wine circles), CGMF (open blue diamonds), FREYA (open green triangles) and the very recent experimental data of Göök *et al.* [3] (full black squares).

data and the results of FIFRELIN and PbP are visible near symmetric fission.

The PbP model result of $\langle\varepsilon\rangle(A)$ of ^{235}U(n_{th}, f) is given with full red circles in fig. 9 together with the results of three Monte Carlo prompt emission codes (inter-compared in ref. [1]): FIFRELIN (open wine circles), CGMF (open blue diamonds) and FREYA (open green triangles).

The experimental data of Göök *et al.*, plotted in fig. 9 with full black squares, were reported very recently [3], *i.e.* after the model calculations were performed.

As can be seen, the best agreement with these new experimental data is realized by the PbP model result. This fact proves the capability of prediction of the PbP model.

In fig. 10 the PbP result of the energy carried away per neutron as a function of A for ^{252}Cf(SF), calculated according to eq. (11), is plotted with full red circles in comparison with the experimental data of Nifenecker *et al.* [23] (open circles).

As can be seen the PbP result describes well the experimental data over the entire A range except for $90 < A < 100$ and $A \sim 130$. This agreement can be also considered as an indirect validation of the average neutron separation energy from fragments resulting from sequential emission (which enters the expression of η, eq. (11)), taking into account that $\langle\varepsilon\rangle$ is already validated (see fig. 8).

The experimental average prompt γ-ray energy of a fragmentation as a function of A_H of ^{252}Cf(SF) reported by Nifenecker *et al.* [23] (black squares) are well described by the PbP result (red circles) as can be seen in fig. 11.

The PbP result of $\langle E_\gamma\rangle(A)$ of ^{235}U(n_{th}, f) (red circles) is in good agreement with the data of Pleasonton *et al.* [33] (black squares), see fig. 12. A previous PbP result [14] (blue stars) when only 2 charge numbers Z per A were considered in the construction of the fragmentation range is given for comparison.

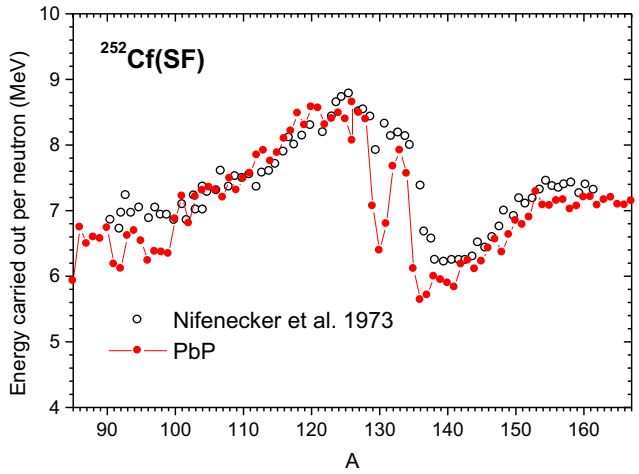

Fig. 10. The energy carried away per neutron (according to eq. (11)) as a function of A for ^{252}Cf(SF): the data of Nifenecker *et al.* [23] are plotted with open black circles and the PbP result with full red circles.

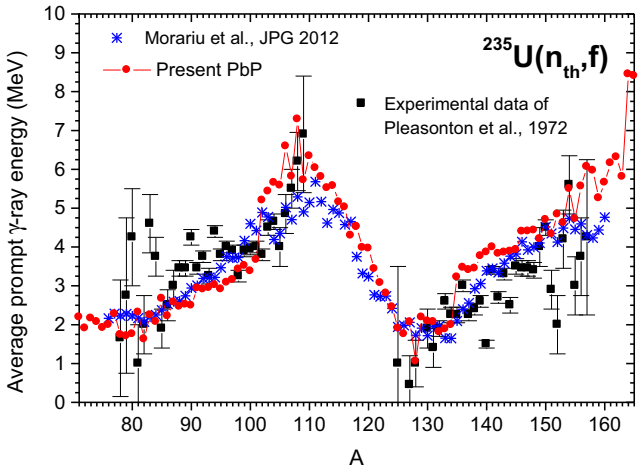

Fig. 12. The average prompt γ-ray energy as a function of A of ^{235}U(n_{th}, f): the present PbP result (red circles) compared with the experimental data of Pleasonton *et al.* [33] (full black squares). The previous PbP results reported in ref. [14] (blue stars) are plotted with blue stars.

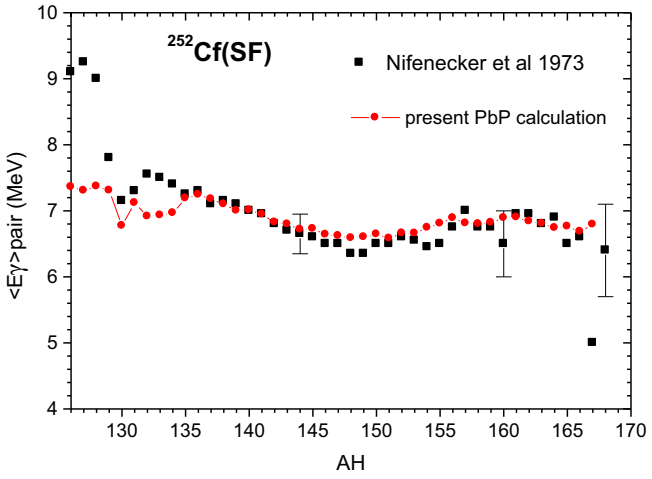

Fig. 11. The PbP result of $\langle E_\gamma \rangle_{pair}$ as a function of A_H (red circles) of ^{252}Cf(SF) in comparison with the data of Nifenecker *et al.* [23] (black squares).

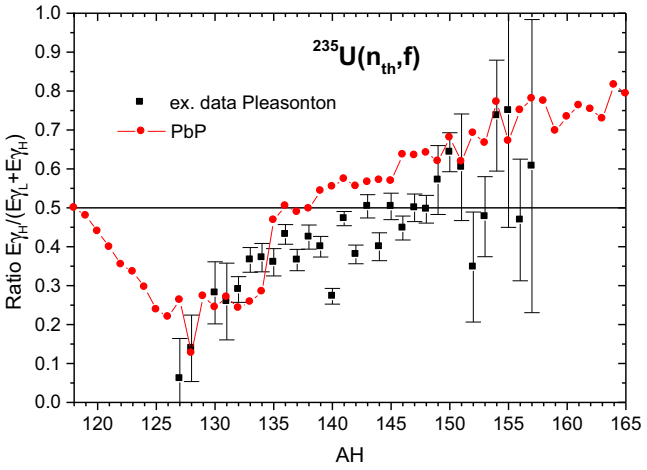

Fig. 13. The ratio $\langle E_\gamma \rangle_H / \langle E_\gamma \rangle_{pair}$ as a function of A_H for ^{235}U(n_{th}, f): the present PbP result (red circles) and the data of Pleasonton *et al.* [33].

In fig. 13 the ratio $\langle E_\gamma \rangle_H / \langle E_\gamma \rangle_{pair}$ is plotted as a function of A_H: the PbP result with red circles and the data of Pleasonton *et al.* [33] with black squares. As can be seen the behaviour of the γ-ray energy ratio is similar to the behaviour of the ν_H/ν_{pair} ratio. *I.e.* the $\langle E_\gamma \rangle_H / \langle E_\gamma \rangle_{pair}$ ratio is less than 0.5 for A_H less than ~ 140 with the lowest values at A_H between 125 and 133, it is of about 0.5 at A_H around 140 and increases at A_H above this value. The experimental data are missing for A_H less than 127. Even if there is a large scatter, a similar trend can be observed.

The prompt fission energy deposition in the medium as a function of A_H, calculated according to the definition of Madland [22], eq. (13), is exemplified in the upper part of fig. 14 for ^{235}U(n_{th}, f). The total average value resulting by averaging this plotted quantity over the fragment distribution (according to eq. (15c)) is $\langle E_d \rangle_{tot} = 180.65$ MeV. This value is in very good agreement with the result reported by Madland [22] where the dependence of this quantity on incident neutron energy is given as $\langle E_d \rangle_{tot} = 180.56 + 0.112 E_n$ (MeV) for the neutron-induced fission of ^{235}U. The prompt fission energy deposition as a function of fragment mass, according to eq. (14), is plotted in the lower part of fig. 14. The average values of the energy deposition of the light and heavy fragment groups are given in the figure, too.

Note, obviously the total average energy deposition $\langle E_d \rangle_{tot}$ can be also obtained as a sum of the total average values of its components, *i.e.* $\langle E_d \rangle_{tot} = \langle Q \rangle_{tot} + B_n + E_n - \langle \nu \rangle_{tot} \langle S_n \rangle_{tot}$. An obtained $\langle E_d \rangle_{tot}$ value close to the value reported in ref. [22] is not surprising because the present total average values: $\langle Q \rangle = 186.79$ MeV, $\langle S_{n_L} \rangle = 5.3325$ MeV, $\langle S_{n_H} \rangle = 4.7466$ MeV, $\langle \nu_L \rangle = 1.3505$, $\langle \nu_H \rangle = 1.1291$ are also close to the values reported by Madland and Kahler in ref. [6]: $\langle Q \rangle = 187$ MeV, $\langle S_{n_L} \rangle =$

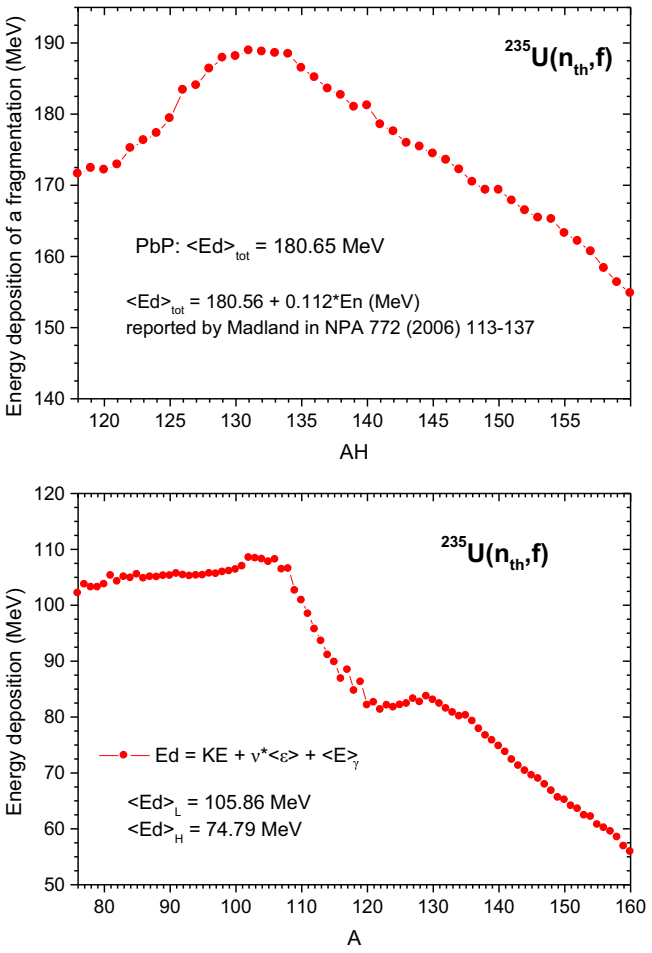

Fig. 14. Prompt fission energy deposition in the medium for $^{235}\mathrm{U}(n_{th}, f)$. Upper part: the prompt energy deposition of a fragmentation according to eq. (13) plotted as a function of A_H. Lower part: the prompt energy deposition of a fragment according to eq. (14). The average values of the prompt energy deposition corresponding to the light and heavy fragment groups and the total average value are given in the figure, too.

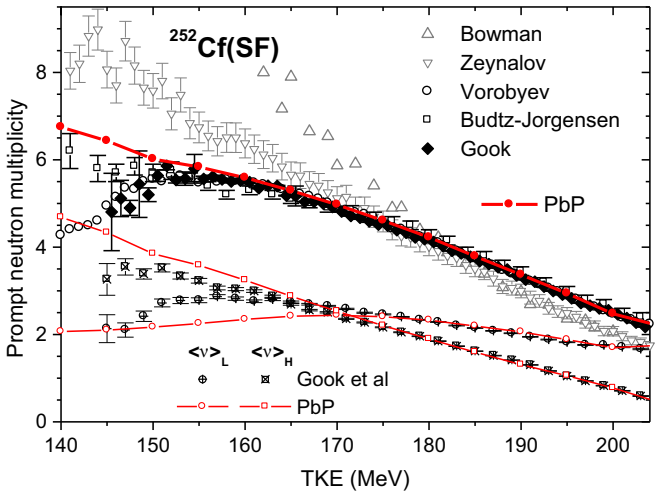

Fig. 15. The PbP result of $\langle\nu\rangle(TKE)$ for ^{252}Cf(SF) (full red circles) in comparison with earlier experimental data sets (different open symbols) and the data of Göök *et al.* [2]. The PbP results of $\langle\nu_L\rangle(TKE)$ (open red circles) and of $\langle\nu_H\rangle(TKE)$ (open red squares) are given in comparison with the data of Göök *et al.* (black circles and squares with a cross inside, respectively).

5.338 MeV, $\langle S_{n_H}\rangle = 4.658$ MeV, $\langle\nu_L\rangle = 1.30 \pm 0.13$, $\langle\nu_H\rangle = 1.13 \pm 0.11$.

Other quantities as a function of A, *e.g.* the fragment excitation energy at full acceleration $E^*(A)$, the fragment level density parameter $a(A)$ of different level density prescriptions, the maximum temperature $T_m(A)$ of the residual temperature distribution were already reported (*e.g.* refs. [9,15,16] and references therein).

3.3 Average quantities as a function of TKE

The available data in the literature on the TKE dependence of the prompt neutron multiplicity show strong deviations and different decreasing slopes.

For ^{252}Cf(SF) different data sets exhibit very different inverse slopes $(\mathrm{d}\nu/\mathrm{d}TKE)^{-1}$, see the open symbols in fig. 15. The work of Göök *et al.* [2] focused on the investigation of experimental factors in low-efficiency neutron-counting experiments that may lead to a faulty determination of this dependence. Taking these factors into account, the $\langle\nu\rangle(TKE)$ result of ref. [2], plotted in fig. 15 with full black diamonds, agrees well with the data from high-efficiency neutron counting experiments.

The PbP result of $\langle\nu\rangle(TKE)$ of ^{252}Cf(SF) obtained by averaging the matrix $\nu(A, TKE)$ over the $Y(A, TKE)$ distribution of Göök *et al.* (according to eq. (15b)) is plotted in fig. 15 with full red circles connected with a solid line. It describes well the data of Göök (full black diamonds), Budtz-Jorgensen and Knitter [30] (open black squares) and Vorobyev *et al.* taken from EXFOR [34] over the entire TKE range except the low TKE values below 150 MeV where the PbP result does not reproduce the decrease exhibited by the data of Göök and Vorobyev.

As expected the PbP results of $\langle\nu_L\rangle(TKE)$ and $\langle\nu_H\rangle(TKE)$ (open red circles and squares) describes well the data of Göök *et al.* (black circles and squares with a cross inside) at TKE above 160 MeV. The data of Budtz-Jorgensen do not show the pronounced decrease at low TKE values exhibited by the data of Göök and Vorobyev. Consequently, the PbP result agrees with the data of Budtz-Jorgensen over the entire TKE range.

Note, the $\langle\nu\rangle(TKE)$ result of the FIFRELIN code [35], as well as the results of other MC codes, also does not show a decrease at low TKE values neither for ^{252}Cf(SF) nor for other fissioning nuclei.

The PbP result of the average prompt neutron energy in the center-of-mass frame as a function of TKE of ^{252}Cf(SF), plotted with red circles in fig. 16, is in good agreement with the experimental data of Nifenecker *et al.* [36] (full black squares). The data of Bowman *et al.* [37] (open circles) are lower than the data of Nifenecker and the PbP result at TKE values from about 165 MeV to 195 MeV.

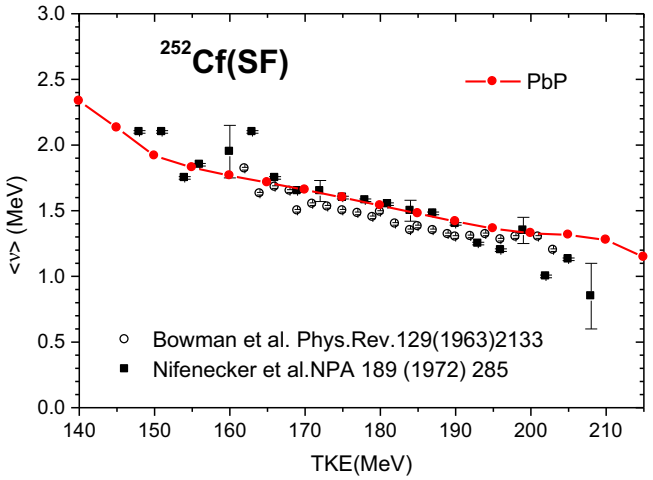

Fig. 16. $\langle\varepsilon\rangle(TKE)$ of ^{252}Cf(SF): the PbP result (full red circles) in comparison with the experimental data of Nifenecker *et al.* (full black squares) and of Bowman *et al.* (open circles).

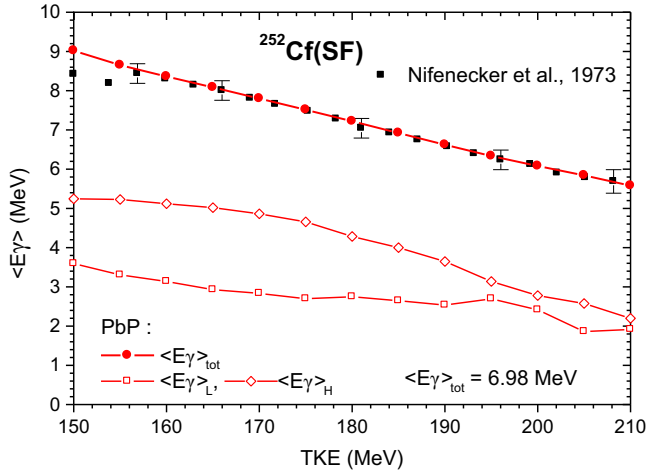

Fig. 17. The PbP results of $\langle E_\gamma\rangle(TKE)$ for ^{252}Cf(SF) (red symbols) in comparison with the data of Nifenecker *et al.*, 1973 [23] (black squares).

The PbP result of the average prompt γ-ray energy as a function of TKE of ^{252}Cf(SF) (full red circles) is in excellent agreement with the data of Nifenecker *et al.* [23] (black squares) as can be seen in fig. 17. The PbP result of $\langle E_\gamma\rangle(TKE)$ averaged over the $Y(TKE)$ distribution of Göök *et al.* gives the total average value $\langle E_\gamma\rangle_{tot} = 6.98$ MeV in very good agreement with the majority of experimental data giving values of about 7 MeV.

The linear correlation between the prompt neutron multiplicity and prompt γ-ray energy is illustrated in fig. 18: the experimental data of Nifenecker *et al.* [23] (full black squares) are very well described by the correlation (plotted with red circles) obtained from the PbP results of $\langle\nu\rangle(TKE)$ and $\langle E_\gamma\rangle(TKE)$ (given in figs. 15 and 17, respectively).

The PbP result of $\langle\nu\rangle(TKE)$ for ^{235}U(n_{th}, f) is plotted in fig. 19 with full red circles connected with solid lines together with the results of the Monte Carlo prompt emission codes FIFRELIN (blue line), CGMF (green line) and FREYA (dark yellow line) reported in ref. [1]. The very recent data of Göök *et al.* [3] are plotted with full black squares.

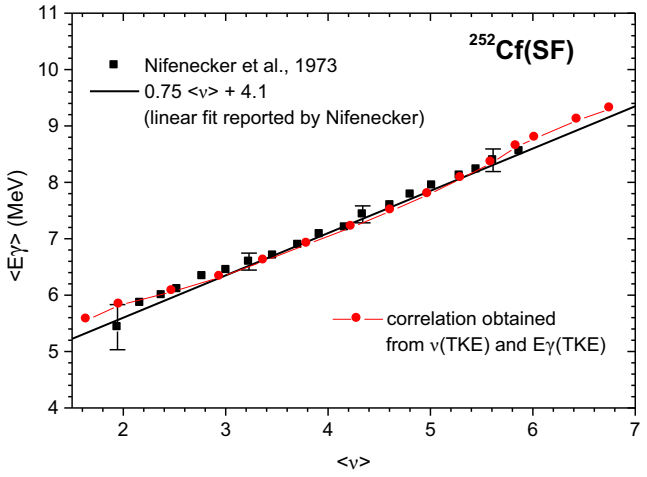

Fig. 18. The linear correlation between the prompt neutron multiplicity and prompt γ-ray energy for ^{252}Cf(SF). The experimental data of Nifenecker *et al.* are plotted with black squares. The linear fit reported by Nifenecker *et al.* is given with a black line. The correlation obtained from the PbP results of $\langle\nu\rangle(TKE)$ and $\langle E_\gamma\rangle(TKE)$ is plotted with red circles.

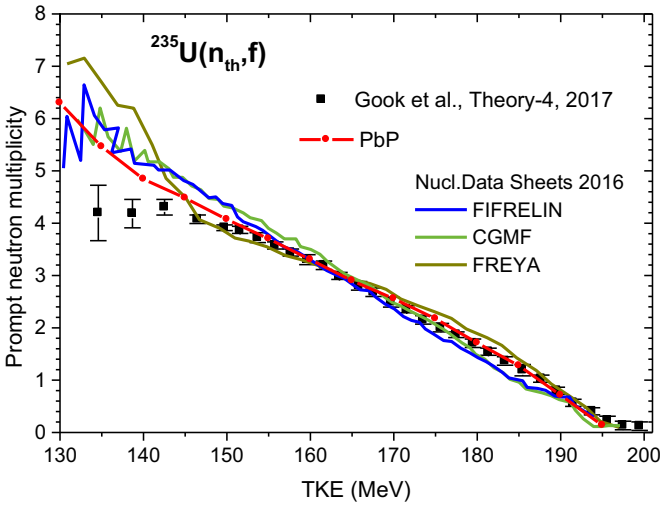

Fig. 19. $\langle\nu\rangle(TKE)$ of ^{235}U(n_{th}, f): the PbP result (red circles connected with solid lines) and the results of the MC computer codes FIFRELIN (blue line), CGMF (green line) and FREYA (dark yellow line) reported in ref. [1] in comparison with the very recent data of Göök *et al.* [3] (full black squares).

As can be seen all model calculations exhibit similar decreasing slopes. However it is easy to see that the PbP result gives the best description of the recent experimental data of Göök *et al.* [3].

Note, again all $\langle\nu\rangle(TKE)$ calculations given in this figure were predictions, being performed before the data of Göök *et al.* became available. Consequently, the excellent agreement of the PbP result with the recent experimental

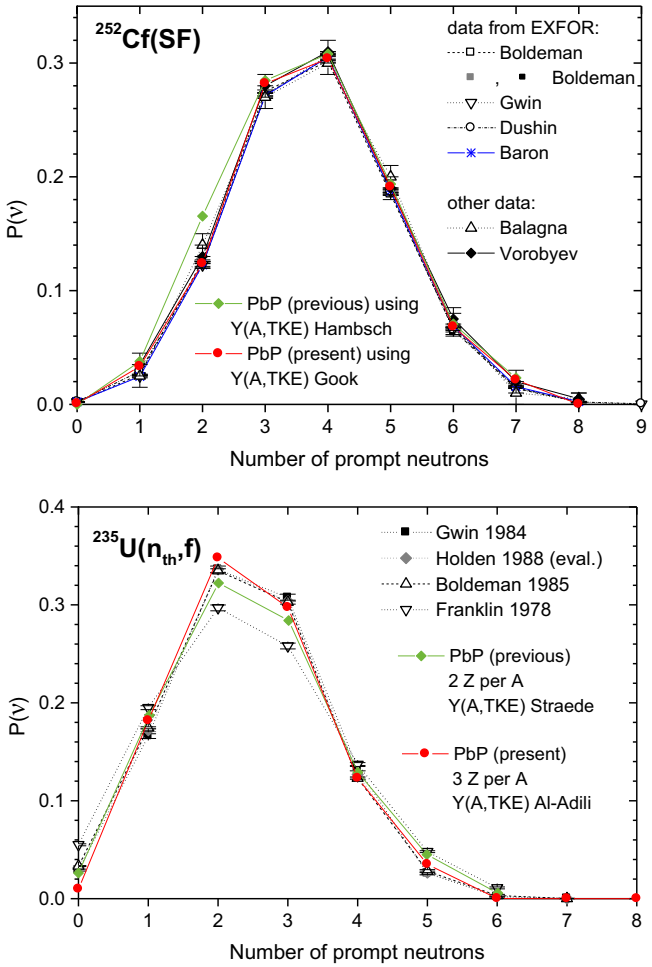

Fig. 20. The prompt neutron distribution $P(\nu)$ of ^{252}Cf(SF) (upper part) and ^{235}U(n_{th}, f) (lower part). The present PbP result is plotted with red circles, the previous result reported in ref. [25] is given with green diamonds. The experimental data sets taken from EXFOR are plotted with different black and gray symbols.

data of Göök *et al.* proves again the capability of prediction of the PbP model.

3.4 Prompt neutron distribution P(ν)

The comparison of the prompt neutron distribution $P(\nu)$ with the experimental data is important because this quantity is very sensitive to both the matrix of prompt neutron multiplicity $\nu(A, Z, TKE)$, as primary result reflecting the model performances, and the multiple fragment distributions $Y(A, Z, TKE)$.

The present $P(\nu)$ results of ^{252}Cf(SF) and ^{235}U(n_{th}, f) are plotted with full red circles in the upper and lower part of fig. 20, respectively, in comparison with all experimental $P(\nu)$ data found in EXFOR [38] and literature (given with different black and gray symbols). Previous $P(\nu)$ results reported in ref. [25] are also given for comparison. They were obtained by averaging the $\nu(A, Z, TKE)$ matrix over the fragment distributions available at that time (*i.e.* of Hambsch and Oberstedt [39] for ^{252}Cf(SF) and of Straede *et al.* [31] for ^{235}U(n_{th}, f)). Also the fragmentation ranges used in the previous PbP calculations of ref. [25] was constructed by taking only 2 charge numbers Z at each A and considering the same $\Delta Z = |0.5|$ and $rms = 0.6$ for all fragmentations.

It is easy to see that the present $P(\nu)$ results, based on the more recent fragment distributions of refs. [2,4] and on fragmentations ranges built by taking 3 charge numbers Z per A with ΔZ and rms as a function of A, describe better the experimental data than the previous results reported in ref. [25]. The values of the total average prompt neutron multiplicity resulting from $P(\nu)$ as

$$\langle\nu\rangle_{tot} = \sum_{\nu} \nu P(\nu) \Big/ \sum_{\nu} P(\nu) \qquad (16)$$

are given in table 1 (for both, the experimental data sets and the PbP results). As can be seen, for both fissioning nuclei the $\langle\nu\rangle_{tot}$ values of PbP are in agreement with the experimental values and they are also close to the standard values of ENDF (*i.e.*, 3.759 for ^{252}Cf(SF) and 2.42 for ^{235}U(n_{th}, f)).

3.5 Total average prompt fission neutron spectra

Because model results and evaluations of the prompt fission neutron spectrum (PFNS) were the objective of the recent comprehensive paper [1], in this section we give only results in connection with the very recent Los Alamos model with non-equal T_m of Madland and Kahler [6].

In the PbP treatment the total average prompt fission neutron spectra in the laboratory frame, $N_{tot}(E)$, are obtained by averaging the prompt neutron spectra of fragment pairs, $N_{pair}(E)$ over the fragment distributions $Y(A, Z, TKE)$ according to eq. (15c).

An example of PbP calculation of PFNS is plotted for ^{235}U(n_{th}, f) in the upper part of fig. 21 in comparison with the experimental data of Vorobyev and Shcherbakov [40] used by Madland and Kahler in ref. [6]. A good description of experimental data was obtained ($\chi^2 = 0.654$).

Note, in this figure and in the next one, the experimental spectrum data were each time re-normalized to the respective spectrum calculation. All PFNS are given in the traditional representation as a ratio to a Maxwellian spectrum with the temperature parameter TM indicated in the legend of the vertical axis.

The improved version of the LA model, recently reported by Madland and Kahler [6], consists in the consideration of non-equal maximum temperatures T_m (of the residual $P(T)$ distribution given by eq. (6)) for the light and heavy fragments of the most probable fragmentation, similar to the PbP model in which, for each fragmentation, the T_m values are given by eq. (7).

The paper of Madland and Kahler [6] demonstrates the good performance of this improved LA model when it uses input model parameters provided by an interesting procedure based on the analytical expression of the average neutron energy $\langle E\rangle$ (first-order momentum of $N_{tot}(E)$) obtained in the approximation of a constant $\sigma_c(\varepsilon)$. This $\langle E\rangle$

Table 1. $\langle\nu\rangle_{tot}$ resulting from $P(\nu)$.

^{252}Cf(SF)		^{235}U(n_{th}, f)	
$P(\nu)$ data	$\langle\nu\rangle_{tot}$	$P(\nu)$ data	$\langle\nu\rangle_{tot}$
Boldeman (exp.)	3.7570 ± 0.0111	Gwin (exp.)	2.4368 ± 0.0183
Boldeman (exp.)	3.7566 ± 0.0111	Holden (exp.)	2.4132 ± 0.0212
Boldeman (exp.)	3.7571 ± 0.0140	Boldeman (exp.)	2.4055 ± 0.0136
Gwin (exp.)	3.7733 ± 0.0083	Franklin (exp.)	2.4146 ± 0.0157
Dushin (exp.)	3.756^a	PbP	2.4382
Baron (exp.)	3.7830 ± 0.0246		
Balagna (exp.)	3.7696 ± 0.1225		
Vorobyev (exp.)	3.7847 ± 0.1195		
PbP	3.7661		

[a] the EXFOR entry of this data set does not contain information about uncertainties.

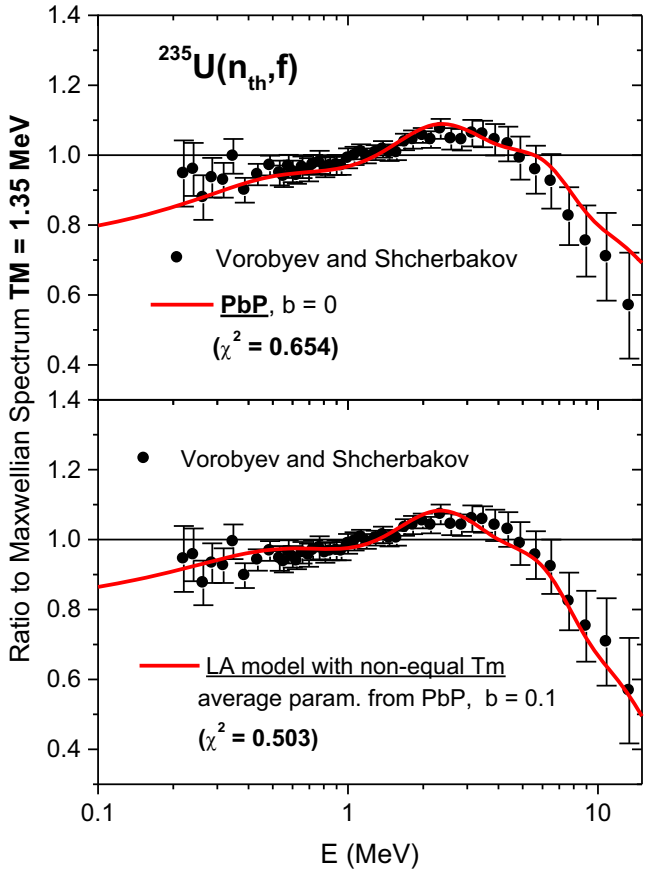

Fig. 21. PFNS of ^{235}U(n_{th}, f) as ratio to a Maxwellian spectrum with $TM = 1.35$ MeV in comparison with the data of Vorobyev and Shcherbakov. Upper part: the PbP result. Lower part: the results of the LA model with non-equal T_m with the average model parameters resulting from the PbP treatment and an anisotropy parameter $b = 0.10$.

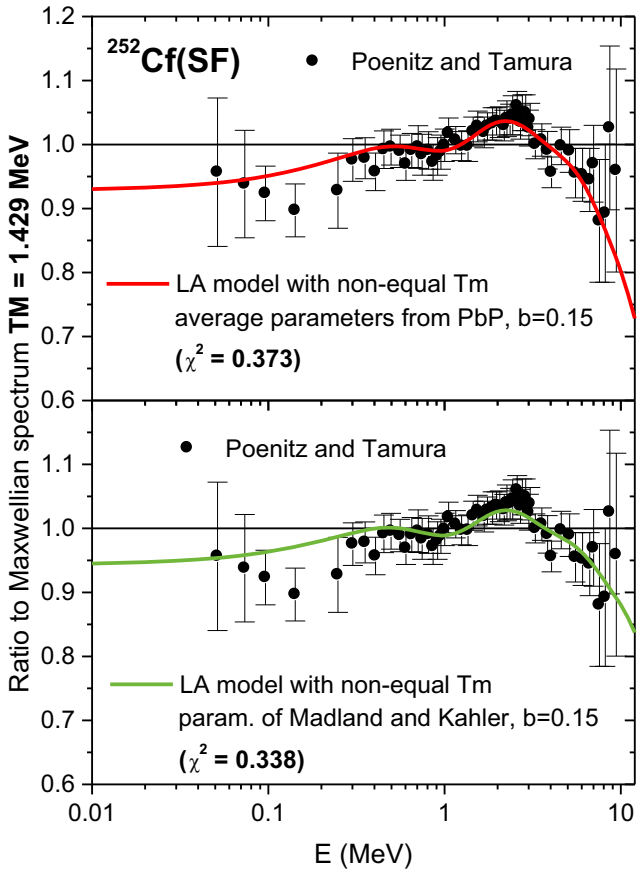

Fig. 22. PFNS result of the LA model with non-equal T_m for ^{252}Cf(SF) given as ratio to a Maxwellian spectrum with $TM = 1.429$ MeV in comparison with the data of Poenitz and Tamura. The calculation is done with the average parameters from the PbP treatment (upper part) and the parameters of Madland and Kahler (lower part). In both cases $b = 0.15$.

value, differing less than 7% from the value obtained when $\sigma_c(\varepsilon)$ from optical model calculations is used, allows to obtain the average level density parameters a_L and a_H of the light and heavy fragment of the most probable fragmentation. The average multiplicity and prompt γ-ray energy corresponding to the light and heavy fragment entering

Table 2. Average parameters for the LA model with non-equal T_m obtained from the PbP treatment.

Parameter	^{235}U(n_{th}, f)	^{252}Cf(SF)
$\langle TKE \rangle$ (MeV)	169.40	184.12
$\langle E_L^* \rangle$ (MeV)	11.492	19.991
$\langle E_H^* \rangle$ (MeV)	11.057	15.038
$\langle a_L \rangle$ (MeV^{-1})	11.001	17.474
$\langle a_H \rangle$ (MeV^{-1})	10.809	12.424
$\langle S_{n_L} \rangle$ (MeV)	5.225	5.932
$\langle S_{n_H} \rangle$ (MeV)	4.734	4.976
Most prob. fragm.	^{96}Sr, ^{140}Xe	^{108}Mo, ^{144}Ba

this procedure are obtained from the experimental $\nu(A)$ and $E_\gamma(A)$ data averaged over a fragment distribution.

In other words this procedure to obtain the input parameters of the recent LA model [6] is limited to the fissioning nuclei for which experimental $\nu(A)$ and $E_\gamma(A)$ data exist.

The PbP treatment can also provide the input parameters of the improved LA model of Madland and Kahler [6] by averaging the multi-parametric matrices of the respective quantities (*e.g.* $E^*(A, Z, TKE)$, $a(A, Z, TKE)$ at full acceleration and $\overline{S}_n(A, Z, TKE)$) over the fragment distribution $Y(A, Z, TKE)$ separately for the light and heavy fragment groups.

The fragment weights taken by Madland and Kahler as experimental multiplicity ratios $\langle \nu_{L,H} \rangle / \langle \nu \rangle_{tot}$ are replaced in this case by the average excitation energy ratios of eq. (10).

The average model parameters obtained in this way, as well as the fragment weights based on the fragment excitation energies resulting from modeling at scission, extend the application of the LA model of Madland and Kahler [6] to fissioning nuclei without any experimental information concerning the prompt neutron and γ-ray energy distribution as a function of A.

The application of the LA model with non-equal T_m using the average parameter values resulting from the PbP treatment is illustrated for ^{235}U(n_{th}, f) in the lower part of fig. 21 and for ^{252}Cf(SF) in the upper part of fig. 22.

The average parameter values used in these calculations are listed in table 2.

As can be seen in the lower part of fig. 21, in the case of ^{235}U(n_{th}, f) the description of experimental data is improved compared to the PbP result given in the upper part (*i.e.*, $\chi^2 = 0.503$ *versus* $\chi^2 = 0.654$) by the consideration of anisotropy, with $b = 0.1$.

In the case of ^{252}Cf(SF) the PFNS result of the LA model with non-equal T_m (upper part of fig. 22), obtained with average parameters resulting from the PbP treatment, describes very well ($\chi^2 = 0.373$) the experimental data of Poenitz and Tamura [41] and Blain [42] (also used by Madland and Kahler in ref. [6]).

For comparison the PFNS obtained with the parameters of Madland and Kahler from ref. [6] (which were obtained by the procedure based on experimental $\nu(A)$ and $E_\gamma(A)$ data) is given in the lower part of fig. 22. A very good description of experimental data is obtained, *i.e.* $\chi^2 = 0.338$ *versus* $\chi^2 = 0.373$ for the case of parameters from the PbP treatment.

The good description of experimental data by the spectrum results of the LA model with non-equal T_m, based on average parameters of the light and heavy fragment groups obtained from the PbP treatment demonstrates the possibility to predict the parameters of this new LA model for fissioning nuclei without any experimental information about the prompt neutron multiplicity and prompt γ-ray energy. Solely the PbP treatment is used, with excitation energy partition based on modeling at scission. The unique data needed to obtain the average model parameters of the light and heavy fragment groups are the fragment distributions $Y(A, TKE)$.

4 Conclusions

The experiment of Göök *et al.* [2] regarding the prompt neutron multiplicity in correlation with the fragment mass and TKE of ^{252}Cf(SF) and its fragment distribution $Y(A, TKE)$, together with the very recent experimental investigation of the prompt neutron emission of ^{235}U(n, f) in the resolved resonance region performed by Göök *et al.* [3], as well as other experimental data of prompt emission for ^{252}Cf(SF) and ^{235}U(n_{th}, f) allowed a consistent and detailed validation of the PbP model.

The PbP results succeeded to describe very well a large variety of experimental data, starting from the multi-parametric matrices of prompt neutron multiplicity $\nu(A, TKE)$ and γ-ray energy $\langle E_\gamma \rangle(A, TKE)$, which validate the model itself.

Different average prompt emission data as a function of A (*e.g.*, $\nu(A)$, $E_\gamma(A)$, $\langle \varepsilon \rangle(A)$, $\eta(A)$) and as a function of TKE (*e.g.*, $\nu(TKE)$, $\langle \varepsilon \rangle(TKE)$, $E_\gamma(TKE)$), as well as the prompt neutron distribution $P(\nu)$ and total average prompt neutron spectra, are well reproduced, too.

The PbP model does not use free or adjustable input parameters. To calculate the multi-parametric matrices $q(A, Z, TKE)$ it needs only data included in the reference input parameter library RIPL1-3 of IAEA (*e.g.*, mass excesses, shell corrections, optical model parameterizations adequate for the nuclei appearing as fragments).

The success of the PbP model in the description of different average prompt emission data is due, not only to the model itself, but also to the reliable experimental distributions $Y(A, TKE)$ used to average the PbP multi-parametric matrices.

The results of the PbP deterministic model are also in agreement with the results of the probabilistic prompt emission codes as it was shown in ref. [1] where an inter-comparison of three Monte Carlo codes (FIFRELIN, CGMF, FREYA) and PbP is reported for the fissioning system ^{235}U(n_{th}, f) taken as example.

The good description of a large variety of experimental data proves that the PbP model is powerful and reliable. It can serve in nuclear data evaluations, as it was already done, see ref. [1]. It can predict data for fissioning nuclei and energies for which the experimental information is completely missing. This was already proven by the prediction of $\nu(A)$ for the reactions $n + {}^{235,238}\mathrm{U}$ at incident neutron energies where multiple fission chances are involved, see refs. [43,44]. And it is proven also in the present work by the good prediction of $\langle\nu\rangle(TKE)$ and $\langle\varepsilon\rangle(TKE)$ of ${}^{235}\mathrm{U}(n_{th}, f)$ which was confirmed by the very recent data reported by Göök *et al.* [3].

The PbP treatment can also provide input model parameters of the improved Los Alamos model with non-equal T_m, very recently reported by Madland and Kahler [6], especially for fissioning nuclei without any experimental information concerning the prompt emission.

One of authors (AT) thanks Alf Göök for providing experimental data and for interesting discussions during this work. A part of this work is done in the frame of the Romanian Project PCE-2016-0014.

References

1. R. Capote, Y.J. Chen, F.-J. Hambsch, N.V. Kornilov, J.P. Lestone, O. Litaize, B. Morillon, D. Neudecker, S. Oberstedt, T. Ohsawa, N. Otuka, V.G. Pronyaev, A. Saxena, O. Serot, O.A. Shcherbakov, N.C. Shu, D.L. Smith, P. Talou, A. Trkov, A.C. Tudora, R. Vogt, S. Vorobyev, Nucl. Data Sheets **131**, 1 (2016).
2. A. Göök, F.-J. Hambsch, M. Vidali, Phys. Rev. C **90**, 064611 (2014).
3. A. Göök, F.-J. Hambsch, S. Oberstedt, *Prompt fission neutron emission in the reaction* ${}^{235}U(n, f)$, in *THEORY-4 Scientific Workshop on Nuclear Fission Dynamics and the Emission of Prompt Neutrons and Gamma Rays, 20–22 June 2017, Varna, Bulgaria*, to be published in EPJ Web of Conferences.
4. A. Al-Adili, F.-J. Hambsch, S. Pomp, S. Oberstedt, Phys. Rev. C **86**, 054601 (2012).
5. D.G. Madland, J.R. Nix, Nucl. Sci. Eng. **81**, 213 (1982).
6. D.G. Madland, A.C. Kahler, Nucl. Phys. A **957**, 289 (2017).
7. A. Tudora, Ann. Nucl. Energy **36**, 72 (2009).
8. A.C. Wahl, At. Data Nucl. Data Tables **39**, 1 (1988).
9. A. Tudora, F.-J. Hambsch, S. Oberstedt, G. Giubega, I. Visan, Nucl. Sci. Eng. **181**, 289 (2015).
10. A. Tudora, F.-J. Hambsch, G. Giubega, I. Visan, Nucl. Phys. A **929**, 260 (2014).
11. A. Tudora, F.-J. Hambsch, G. Giubega, I. Visan, Nucl. Phys. A **933**, 165 (2015).
12. A. Tudora, F.-J. Hambsch, G. Giubega, Eur. Phys. J. A **52**, 182 (2016).
13. R. Capote, M. Herman, P. Oblozinsky, P.G. Young, S. Goriely, T. Belgya, A.V. Ignatiuk, A.J. Koning, S. Hilare, V.A. Plujko, M. Avrigeanu, O. Bersillon, M.B. Chadwick, T. Fukahory, Zhigang Ge, Yinlu Han, S. Kailas, J. Kopecky, V.M. Maslov, G. Reffo, M. Sin, E.Sh. Soukhovitskii, P. Talou, Nucl. Data Sheets **110**, 3107 (2009) IAEA-RIPL3 electronic library, available online at `https://www-nds.iaea.org`, Segment 1 "Nuclear masses and deformations", the database of Audi and Wapstra.
14. C. Morariu, A. Tudora, F.-J. Hambsch, S. Oberstedt, C. Manailescu, J. Phys. G: Nucl. Part. Phys. **39**, 055103 (2012).
15. A. Tudora, F.-J. Hambsch, I. Visan, G. Giubega, Nucl. Phys. A **940**, 242 (2015).
16. C. Manailescu, A. Tudora, F.-J. Hambsch, C. Morariu, S. Oberstedt, Nucl. Phys. A **867**, 12 (2011).
17. O. Bersillon, *SCAT2 optical model code*, NEA-Data Bank, Computer Program Service, Package NEA 0829/07 version 2010 (V. Manea, University of Bucharest) `http://www.oecd-nea.fr/databank/`.
18. R. Capote, M. Herman, P. Oblozinsky, P.G. Young, S. Goriely, T. Belgya, A.V. Ignatiuk, A.J. Koning, S. Hilare, V.A. Plujko, M. Avrigeanu, O. Bersillon, M.B. Chadwick, T. Fukahory, Zhigang Ge, Yinlu Han, S. Kailas, J. Kopecky, V.M. Maslov, G. Reffo, M. Sin, E.Sh. Soukhovitskii, P. Talou, Nucl. Data Sheets **110**, 3107 (2009) IAEA-RIPL3 electronic library, available online at `https://www-nds.iaea.org`, Segment 4 "Optical model", IREF = 100, Becchetti-Greenlees.
19. F.-J. Hambsch, A. Tudora, G. Vladuca, S. Oberstedt, Ann. Nucl. Energy **32**, 1032 (2005).
20. A. Tudora, F.-J. Hambsch, *Parameterization of the residual temperature distribution based on the modeling of successive emission of prompt neutrons*, in *THEORY-4 Scientific Workshop on Nuclear Fission Dynamics and the Emission of Prompt Neutrons and Gamma Rays, 20–22 June 2017, Varna, Bulgaria*, to be published in EPJ Web of Conferences.
21. J. Terrel, Phys. Rev. **113**, 527 (1959).
22. D.G. Madland, Nucl. Phys. A **772**, 113 (2006).
23. H. Nifenecker, C. Signarbieux, R. Babinet, J. Poitou, *Neutron and gamma emission in fission*, IAEA-SM-174/207 117 review paper (1973).
24. A. Tudora, Ann. Nucl. Energy **35**, 1 (2008).
25. A. Tudora, F.-J. Hambsch, Ann. Nucl. Energy **37**, 771 (2010).
26. A.V. Ignatiuk, in IAEA-RIPL1-TECDOC-1034, Segment V (1998) Chapt. 5.1.4.
27. R. Capote, M. Herman, P. Oblozinsky, P.G. Young, S. Goriely, T. Belgya, A.V. Ignatiuk, A.J. Koning, S. Hilare, V.A. Plujko, M. Avrigeanu, O. Bersillon, M.B. Chadwick, T. Fukahory, Zhigang Ge, Yinlu Han, S. Kailas, J. Kopecky, V.M. Maslov, G. Reffo, M. Sin, E.Sh. Soukhovitskii, P. Talou, Nucl. Data Sheets **110**, 3107 (2009) IAEA-RIPL3 electronic library, available online at `https://www-nds.iaea.org`, Segment 1 "Nuclear masses and deformations", the database of Möller and Nix (FRDM).
28. M. Chadwick *et al.*, Nucl. Data Sheets **112**, 2887 (2011).
29. A. Tudora, F.-J. Hambsch, S. Oberstedt, G. Giubega, I. Visan, Phys. Proc. **59**, 95 (2014).
30. C. Budtz-Jorgensen, H.H. Knitter, Nucl. Phys. A **490**, 307 (1988).
31. Ch. Straede, C. Budtz-Jorgensen, H.H. Knitter, Nucl. Phys. A **462**, 85 (1987).
32. O. Litaize, O. Serot, L. Berge, Eur. Phys. J. A **51**, 177 (2015).
33. F. Pleasonton, R.L. Ferguson, H.W. Schmitt, Phys. Rev. C **6**, 1023 (1972).

34. EXFOR Experimental Nuclear Data Library (available online at `https://www-nds.iaea.org`) nucleus ^{252}Cf, reaction $(0, f)$, quantity MFQ, entry 41425 (Vorobyev).
35. O. Litaize, O. Serot, Phys. Rev. C **82**, 054616 (2010).
36. H. Nifenecker, C. Signarbieux, M. Ribrag, J. Poitou, J. Matuszek, Nucl. Phys. A **189**, 285 (1972).
37. H.R. Bowman, J.C.D. Milton, S.G. Thompson, W.J. Swiateki, Phys. Rev. **129**, 2133 (1963).
38. EXFOR Experimental Nuclear Data Library (available online at `https://www-nds.iaea.org`), nucleus ^{252}Cf, reaction $(0, f)$, quantity MFQ ($P(\nu)$), entry 307720151-3 (J.W. Boldeman *et al.*), entry 12833005 (R. Gwin *et al.*), entry 41425002 (A.S. Vorobyev *et al.*), entry 21495003 (E. Baron *et al.*).
39. F.-J. Hambsch, S. Oberstedt, Nucl. Phys. A **617**, 347 (1997).
40. A.S. Vorobyev, O.A. Shcherbakov, Yad. Konst. **1-2**, 37 (2011-2012).
41. W.P. Poenitz, T. Tamura, *Proceedings of the International Conference on Nuclear Data for Science and Technology, Antwerpen, Belgium 1982*, edited by K.H. Bhockhoff (D. Reidel Publ. Company, Dordrecht, 1983) p. 465.
42. E. Blain, PhD Thesis, Rensselaer Institute, Troy, NY, December 2014.
43. A. Tudora, F.-J. Hambsch, V. Tobosaru, Phys. Rev. C **94**, 044601 (2016).
44. A. Tudora, F.-J. Hambsch, V. Tobosaru, *PbP model calculation of the prompt neutron distribution $\nu(A)$ at incident neutron energies where multiple fission chances are involved*, in *ND-2016, International Conference on Nuclear Data for Science and Technology, Brugge, Belgium, 11-16 September 2016*, to be published in EPJ Web of Conferences.